Rocketdyne R-8151



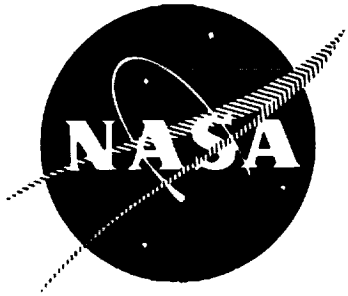


# FINAL REPORT
# SPACE STORABLE PROPELLANT
# VACUUM PERFORMANCE EVALUATION

By
B. J. Waldman

NATIONAL AERONAUTICS AND SPACE ADMINISTRATION
Contract NAS7-741

ROCKETDYNE
North American Rockwell Corporation
6633 Canoga Avenue, Canoga Park, California

NOTICE

This report was prepared as an account of Government sponsored work. Neither the United States, nor the National Aeronautics and Space Administration (NASA), nor any person acting on behalf of NASA:

A.) Makes any warranty or representation, expressed or implied, with respect to the accuracy, completeness, or usefulness of the information contained in this report, or that the use of any information, apparatus, method, or process disclosed in this report may not infringe privately owned rights; or

B.) Assumes any liabilities with respect to the use of, or for damages resulting from the use of any information, apparatus, method or process disclosed in this report.

As used above, "person acting on behalf of NASA" includes any employee or contractor of NASA, or employee of such contractor, to the extent that such employee or contractor of NASA or employee of such contractor prepares, disseminates, or provides access to, any information pursuant to his employment or contractor with NASA, or his employment with such contractor.

Requests for copies of this report should be referred to

National Aeronautics and Space Administration
Office of Scientific and Technical Information
Attention: AFSS-A
Washington, D.C. 20546

# FINAL REPORT
# SPACE STORABLE PROPELLANT
# VACUUM PERFORMANCE EVALUATION

By

B. J. Waldman

Advanced Systems

Technically Reviewed and Approved by

J. Friedman
Program Manager
Small Engine Division

March 1970

## FOREWORD

This report presents the final results of an experimental program titled Space Storable Propellant Vacuum Performance Evaluation. The contract, NAS7-741,was conducted by Rocketdyne, a Division of North American Rockwell Corporation, and was directed for the Jet Propulsion Laboratory by W. B. Powell and for the National Aeronautics and Space Administration by J. Suddreth.

## ABSTRACT

This report covers work performed under the Space Storable Propellant Vacuum Performance Evaluation Program, a research effort conducted under JPL/NASA Contract NAS7-741. During this program rocket engine tests with the propellant combination oxygen difluoride/diborane ($OF_2/B_2H_6$) were conducted in an altitude simulation facility. Performance and heat transfer data were recorded for three different injector configurations.

## ACKNOWLEDGEMENT

Major contributions to the performance of this program were made by the following Rocketdyne personnel:

Mr. A. W. Huebner was the Development Engineer and contributed to the preparation of the final report.

Mr. L. H. Dodgion was the Nevada Field Laboratory Test Engineer.

TABLE OF CONTENTS

ILLUSTRATIONS

# TABLES

# INTRODUCTION

One of the most difficult problems in the prediction of rocket engine performance is the effect of injector design variables on high area ratio nozzle performance (specific impulse and heat transfer). For $OF_2/B_2H_6$, a propellant combination with great promise for high area ratio space propulsion applications, no data were available to correlate injector design with nozzle performance. In addition, the complex chemistry of this propellant makes analytical predictions unreliable.

Several programs had been conducted on the subject of injector-combustor compatibility and performance, Refs. 1 through 3. Most significant was NAS7-304, Space Storable Thrust Chamber Technology Program. One program has been conducted on high area ratio nozzle performance, NASw-1229, Ref. 4. The objective of this present program was to combine the injector design features developed for combustor compatibility with a high area ratio nozzle and experimentally determine the high area ratio specific impulse and nozzle heat transfer.

This program consisted of a brief experimental investigation of injector-nozzle interactions, conducted in Rocketdyne's altitude simulation $OF_2/B_2H_6$ test facility. The basic engine configuration was selected to match the projected requirements for deep space missions planned for the 1980's. The injector configurations were selected to be representative of the types which may eventually be used in a developed propulsion system.

This report summarizes the results of that investigation.

## SUMMARY AND CONCLUSIONS

Experimental thrust chamber firings were conducted with three different injector configurations to establish the effect of injector design on performance and heat transfer in high area ratio engines. Three test series were conducted, one for each injector configuration.

Two injectors were used, one with a stratified mixture ratio design and the other film cooled. The stratified injector used 20 percent of the total mass flow as a barrier at a mixture ratio of 0.5:1. The BLC injector used a swirl injected liquid diborane film consisting of 5-percent and 10-percent of total propellant flowrate.

The thrust chamber was sized for a nominal thrust of 1000 lbf at a chamber pressure of 100 psia. A 15-degree conical nozzle with an area ratio of 60:1 was used. The thrust chamber was a heat sink calorimeter design.

The test program was conducted at the Nevada Field Laboratory Space Engines Area, in the B-3 test capsule. A steam driven hyperflow system was used to create the simulated altitude of 100,000 ft.

Performance results showed the stratified and 5% BLC injectors to be nearly identical in specific impulse performance, both indicating 390 lbf-sec/lbm at mixture ratio of 3:1. The 10% BLC injector produced 372 lbf-sec/lbm at this mixture ratio but at a lower chamber pressure. At equal pressures the performance difference would be more nearly 13 than 18 lbf-sec/lbm.

The heat flux results showed the stratified and 10% BLC to be nearly equal at the throat with a value of 4.5 $BTU/in^2$- sec. The 5% BLC produced about 75% more heat flux, indicating no protection at all in the 10 inch combustion chamber used.

Performance and throat heat flux are summarized in Figure 1 for a mixture ratio of 3:1. Results for NASw-1229 are also shown, although those tests were conducted with gaseous diborane injection and achieved 2-4 percent higher injector efficiencies than obtained in this program with liquid injection.

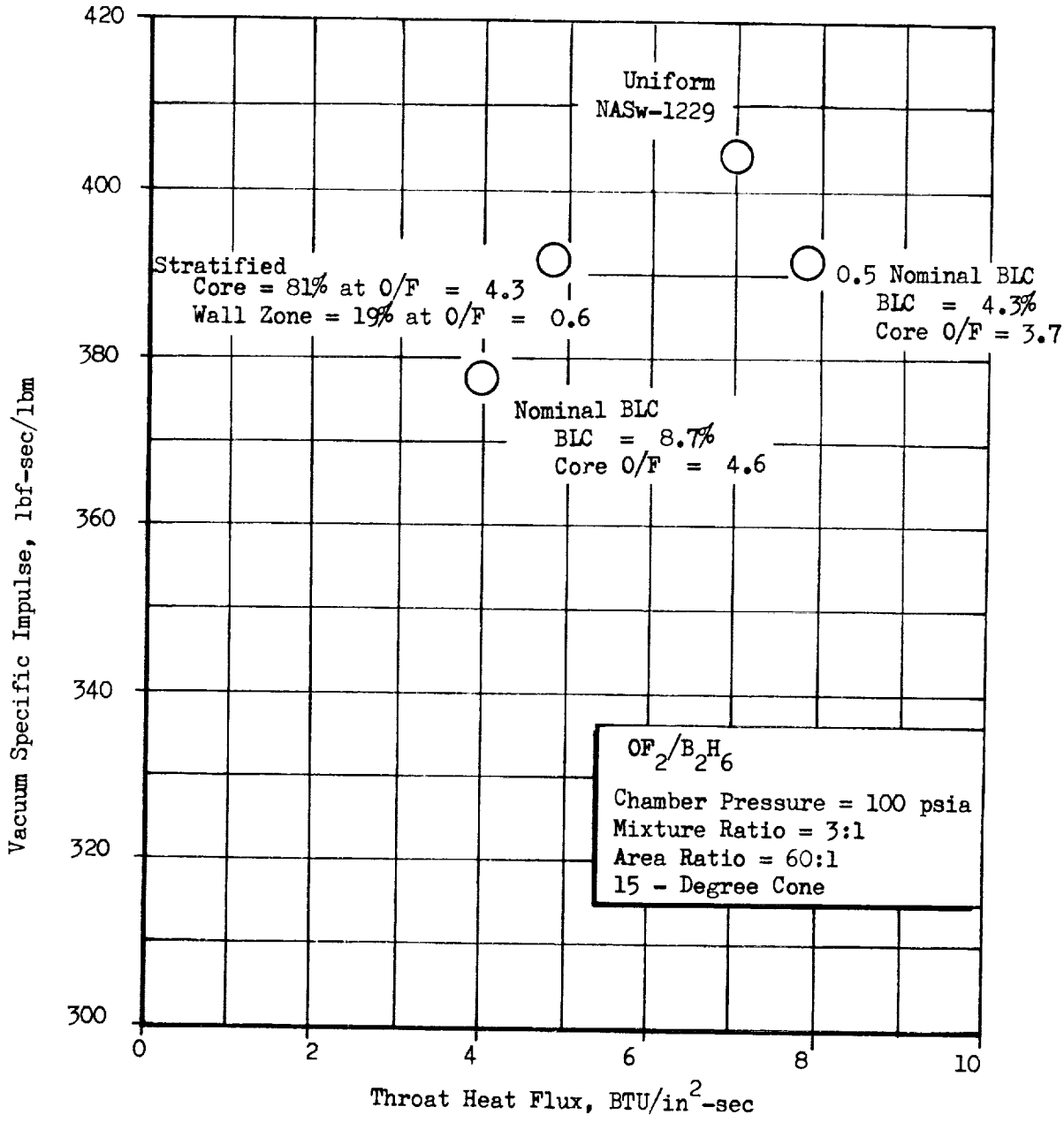


Figure 1. Performance - Heat Flux Comparison for Four Injector Configurations

The performance results confirmed once again that performance indices based on chamber pressure are not necessarily indicative of high area ratio specific impulse performance. In some cases low indicated injector efficiencies were offset by high indicated nozzle performance. Since this condition always makes the data suspect, many forms of consistency checks were employed. However, the results could not be discounted. It is necessary to conclude that either injector design did have an important effect on the relationship between injector and nozzle performance, or that some injector configurations affect the validity with which chamber wall pressure indicates free stream static pressure. Whichever explanation is correct, performance determination for injectors of this type must be based on specific impulse measurement, the objective of this program. However, it is significant that while the variations in injector efficiency were over a range of 15 percent, thrust chamber efficiency varied only about 3 percent. A thrust chamber efficiency value of 93 percent could be used for preliminary design studies with any injector efficiency and probably be within 1 percent of the correct value.

The two different types of injector designs, BLC and stratified, had distinctly different effects on heat flux patterns in the combustion chamber and nozzle. The 10% BLC and stratified injector designs had similar heat flux levels at the throat. The BLC design had much lower heat flux in the combustion chamber as would be expected with the use of a liquid film. However the stratified design produced lower nozzle heat flux by as much as a factor of 2 and provided protection for the nozzle wall to a much higher area ratio.

In this program, the diborane was used at lower temperatures than in most previous tests. The nominal temperature was 250R. After conducting engine tests with the BLC injector which was used with warmer fuel in another program, two new phenomena were observed. The fuel injector pressure drop was excessively higher than measured in the other program, while the oxidizer was in good agreement with previous history. An unusual deposit formation was observed after the 5% BLC test series. No satisfactory explanation has

test facility. Initial injector temperatures varied from 300R to 450R and indicated no effect on pressure drop. The other major difference was the extreme mixture ratios tested in this program. It is possible that the high injector pressure drop caused the deposits. The stratified injector also experienced the high pressure drops.

## TEST RESULTS

The three test series conducted in this project have produced data on performance and heat transfer for three different injector configurations. This section presents the test results and compares them with the results of two other pertinent programs: Space Storable Propellant Technology (NAS7-304, Ref. 1 ) and Space Storable Propellant Performance Investigation (NASw-1229, Ref. 4 ). The basic data for all of the tests are summarized in Table 1.

A diborane flow blockage phenomenon caused many of the tests to be at higher mixture ratios than intended. (Flow blockage is discussed on page 36). Several tests, at least one with each injector configuration, were at useful mixture ratios.

All of the tests were conducted with the same combustion chamber and 15-degree conical nozzle, which are described on page 53. The tests were performed during three vacuum facility operations, one for each injector configuration.

### PERFORMANCE RESULTS

Specific impulse and specific impulse efficiency results for all three injector configurations are summarized in Figs. 2 and 3. Although the mixture ratio range of usual interest centers at 3:1, all of the test results are shown, even at very high mixture ratios. The larger quantity of data points thus made available gives better insight into data trends at the mixture ratios of interest. For reference, the theoretical equilibrium performance curve is shown, as is the mean line of the test results for the 15-degree cone from NASw-1229.

The two film cooled injector configurations (10% and 5% nominal BLC) show a difference of approximately 20 lbf-sec/lbm over the mixture ratio range explored,

| Test No. | | Chamber Wall Pressure psia | Stagnation Pressure $P_c$ psia | | Ambient Throat Area $In^2$ | Pretest Throat Area $In^2$ | Aerodynamic Throat Area $A_T C_D$ $In^2$ | |
|---|---|---|---|---|---|---|---|---|
| 073 | Stratified | 100.10 | 104.95 | | 4.988 | 4.983 | 4.946 | |
| 074 | | 92.04 | 96.50 | | 4.988 | 4.990 | 4.953 | |
| 075 | | 87.42 | 91.66 | | 4.988 | 4.995 | 4.958 | |
| 076 | | 85.95 | 90.12 | | 4.988 | 5.000 | 4.963 | |
| 077 | | 79.44 | 83.29 | | 4.988 | 5.000 | 4.963 | |
| 078 | 10% BLC | 78.97 | 82.82 | | 5.007 | 5.004 | 4.967 | |
| 079 | | 75.64 | 79.31 | | 5.007 | 5.005 | 4.968 | |
| 080 | | 74.89 | 78.52 | | 5.007 | 5.007 | 4.970 | |
| 081 | | 71.04 | 74.48 | | 5.007 | 5.009 | 4.972 | |
| 082 | | 66.07 | 69.30 | | 5.007 | 5.013 | 4.976 | |
| 083 | | 66.94 | 70.19 | | 5.007 | 5.015 | 4.978 | |
| 084 | | 62.74 | 65.78 | | 5.007 | 5.018 | 4.981 | |
| 085 | 5% BLC | 93.04 | 97.55 | | 5.007 | 4.992 | 4.955 | |
| 086 | | 78.66 | 82.48 | | 5.007 | 4.995 | 4.958 | |
| 087 | | 76.03 | 79.72 | | 5.007 | 4.997 | 4.960 | |
| 088 | | 72.25 | 75.75 | | 5.007 | 5.001 | 4.964 | |
| 089 | | 67.85 | 79.31 | | 5.007 | 5.002 | 4.965 | |
| 090 | | 64.43 | 67.55 | | 5.007 | 5.005 | 4.968 | |
| 091 | | 66.16 | 69.37 | | 5.007 | 5.006 | 4.969 | |
| | | | | | | | | |

FOLDOUT FRAME

| Site Thrust $lb_f$ | Capsule Pressure psia | Thrust Correction $lb_f$ | Vacuum Thrust $lb_f$ | | Ox F/M Temp $^oF$ | Ox F/M Press. psia | Ox Flowrate lbm/sec | | Fuel F/M Temp. $^oF$ | Fuel F/M Pr psia |
|---|---|---|---|---|---|---|---|---|---|---|
| 853.4 | .1296 | 39.6 | 993.0 | | -237.6 | 387.2 | 2.012 | | -226.7 | 454. |
| 868.0 | .1005 | 30.6 | 898.6 | | -234.9 | 406.6 | 2.084 | | -224.9 | 475. |
| 818.1 | .0913 | 27.8 | 845.9 | | -233.8 | 419.6 | 2.134 | | -225.6 | 483. |
| 814.6 | .0878 | 26.7 | 841.3 | | -233.6 | 438.1 | 2.193 | | -226.8 | 481. |
| 754.6 | .0819 | 24.9 | 779.5 | | -233.8 | 381.1 | 1.997 | | -225.8 | 484. |
| 753.3 | .0570 | 17.4 | 770.7 | | -194.5 | 306.6 | 1.479 | | -186.7 | 475. |
| 713.1 | .0550 | 16.7 | 729.8 | | -192.6 | 298.4 | 1.478 | | -184.9 | 479. |
| 703.4 | .0752 | 22.9 | 726.3 | | -191.8 | 305.2 | 1.529 | | -184.8 | 482. |
| 667.7 | .0760 | 23.1 | 690.8 | | -191.4 | 322.5 | 1.588 | | -184.1 | 503. |
| 639.4 | .0591 | 18.0 | 657.4 | | -191.5 | 339.7 | 1.683 | | -183.6 | 494. |
| 646.3 | .0533 | 16.2 | 662.5 | | -191.6 | 358.2 | 1.758 | | -182.9 | 496. |
| 596.8 | .0601 | 18.3 | 615.1 | | -191.5 | 320.2 | 1.637 | | -182.4 | 497. |
| 874.2 | .0528 | 16.1 | 890.3 | | -214.2 | 312.8 | 1.794 | | -205.0 | 489. |
| 738.2 | .0458 | 13.9 | 752.1 | | -213.2 | 310.3 | 1.813 | | -204.5 | 504. |
| 719.0 | .0448 | 13.6 | 732.6 | | -212.4 | 340.0 | 1.957 | | -204.1 | 510. |
| 684.3 | .0422 | 12.9 | 697.2 | | -212.5 | 332.9 | - | | -204.3 | 504. |
| 640.5 | .0444 | 13.5 | 654.0 | | -212.1 | 352.9 | 1.962 | | -203.8 | 508. |
| 605.9 | .0472 | 14.3 | 620.2 | | -211.6 | 349.6 | 1.921 | | -202.6 | 514. |
| 624.9 | .0564 | 17.1 | 642.0 | | -210.9 | 368.6 | 1.986 | | -201.8 | 524. |
| | | | | | | | | | | |

FOLDOUT FRAME 7

| Fuel F/M Press psia | Fuel Flowrate lbm/sec | | Total Flowrate lbm/sec | Mixture Ratio O/F | | C* Actual $\frac{P_c A_T C_D g}{\dot{W}}$ ft/sec | C* Theo ft/sec | Injector Efficien- $\eta_{inj}$ |
|---|---|---|---|---|---|---|---|---|
| 454.2 | .568 | | 2.580 | 3.54 | | 6473 | 7137 | 90.7 |
| 475.0 | .372 | | 2.456 | 5.60 | | 6261 | 6967 | 89.9 |
| 483.6 | .298 | | 2.432 | 7.16 | | 6012 | 6785 | 88.6 |
| 481.5 | .302 | | 2.495 | 7.26 | | 5768 | 6775 | 85.1 |
| 484.1 | .258 | | 2.255 | 7.74 | | 5898 | 6718 | 87.8 |
| 475.7 | .581 | | 2.060 | 2.55 | | 6425 | 6953 | 92.4 |
| 479.7 | .480 | | 1.958 | 3.08 | | 6475 | 7066 | 91.6 |
| 482.8 | .461 | | 1.990 | 3.32 | | 6309 | 7095 | 88.9 |
| 503.8 | .356 | | 1.944 | 4.46 | | 6129 | 7075 | 86.6 |
| 494.8 | .284 | | 1.967 | 5.93 | | 5640 | 6907 | 81.7 |
| 496.5 | .265 | | 2.023 | 6.63 | | 5557 | 6835 | 81.3 |
| 497.0 | .245 | | 1.882 | 6.68 | | 5601 | 6830 | 82.0 |
| 489.7 | .508 | | 2.302 | 3.53 | | 6756 | 7130 | 94.8 |
| 504.4 | .297 | | 2.110 | 6.10 | | 6236 | 6905 | 90.3 |
| 510.3 | .247 | | 2.204 | 7.92 | | 5772 | 6693 | 86.2 |
| 504.2 | .267 | | - | - | | - | - | - |
| 508.7 | .209 | | 2.171 | 9.39 | | 5235 | 6520 | 80.3 |
| 514.9 | .203 | | 2.124 | 9.46 | | 5084 | 6508 | 78.1 |
| 524.9 | .203 | | 2.189 | 9.78 | | 5066 | 6470 | 78.3 |
| | | | | | | | | |

FOLDOUT FRAME 3

| $C_f$ Actual | $C_F$ Theo | Thrust Chamber Efficiency $\eta_{TC}$ | | Vacuum Specific Impulse $I_{VAC}$ $lb_f$-sec/$lb_m$ | $I_{VAC}$ Theo | $\eta_{I_{VAC}}$ | | Ox Injection Temp. °F | Fuel Injection Temp. °F | |
|---|---|---|---|---|---|---|---|---|---|---|
| 1.9130 | 2.0025 | 95.5 | | 384.9 | 444.4 | 86.6 | | -222.7 | -187.9 | |
| 1.8800 | 2.0140 | 93.3 | | 365.9 | 436.2 | 83.9 | | -224.6 | - | |
| 1.8614 | 2.0150 | 92.4 | | 347.8 | 424.7 | 81.9 | | -226.2 | - | |
| 1.8810 | 2.0147 | 93.4 | | 337.2 | 424.0 | 79.5 | | -227.0 | - | |
| 1.8857 | 2.0132 | 93.7 | | 345.7 | 419.8 | 82.3 | | -226.1 | - | |
| 1.8735 | 1.9950 | 93.9 | | 374.1 | 433.4 | 86.3 | | -177.8 | -149.8 | |
| 1.8522 | 1.9990 | 92.7 | | 372.7 | 439.8 | 84.7 | | -175.4 | -149.0 | |
| 1.8611 | 2.0010 | 93.0 | | 365.0 | 441.8 | 82.6 | | -178.1 | -148.9 | |
| 1.8654 | 2.0088 | 92.9 | | 355.3 | 441.0 | 80.6 | | -179.7 | -150.1 | |
| 1.9064 | 2.0150 | 94.6 | | 334.2 | 431.2 | 77.5 | | -182.9 | -144.6 | |
| 1.8961 | 2.0155 | 94.1 | | 327.5 | 426.7 | 76.8 | | -184.6 | -141.5 | |
| 1.8773 | 2.0158 | 93.1 | | 326.8 | 426.3 | 76.7 | | -184.1 | -137.8 | |
| 1.8419 | 2.0025 | 92.0 | | 386.8 | 444.0 | 87.1 | | -213.5 | -146.4 | |
| 1.8392 | 2.0115 | 91.3 | | 356.4 | 431.8 | 82.5 | | -213.2 | -150.6 | |
| 1.8528 | 2.0128 | 92.0 | | 332.4 | 418.0 | 79.5 | | -212.2 | -152.3 | |
| 1.8541 | 2.0150 | 92.0 | | - | - | - | | -212.5 | -155.7 | |
| 1.8516 | 2.0054 | 92.3 | | 301.2 | 405.9 | 74.2 | | -211.3 | -158.2 | |
| 1.8481 | 2.0048 | 92.2 | | 292.0 | 405.2 | 72.1 | | -210.6 | -156.1 | |
| 1.8625 | 2.0029 | 93.0 | | 293.3 | 402.7 | 72.8 | | -209.7 | -160.1 | |
| | | | | | | | | | | |

FOLDOUT FRAME 4

Table 1. Test Data Summary

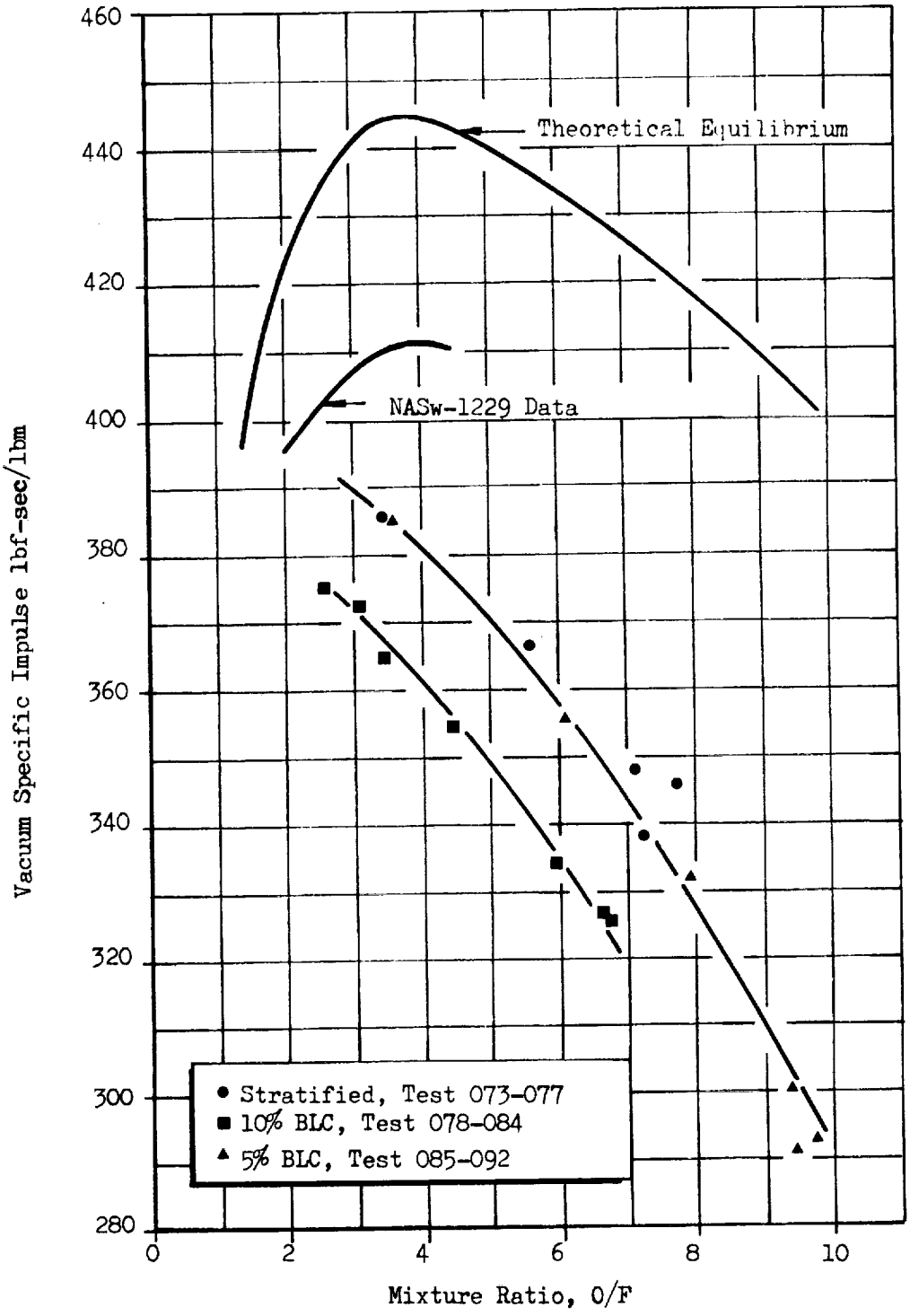


Figure 2. Specific Impulse Test Results

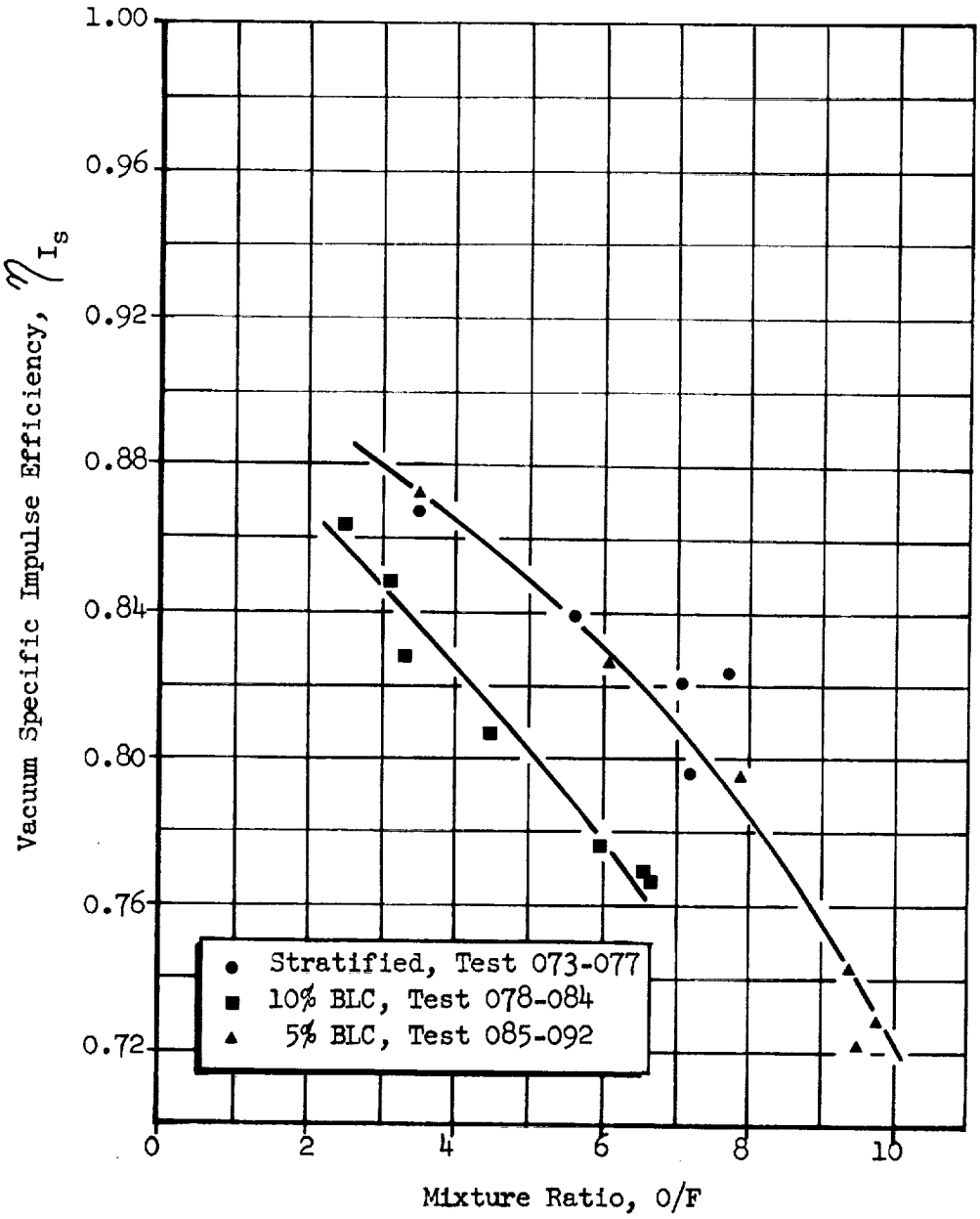


Figure 3. Specific Impulse Efficiency Test Results

with the lower film coolant flowrate producing higher performance, as expected. The stratified flow injector results virtually coincided with the results for 5% nominal BLC.

The low chamber pressures achieved on the 10% BLC test series caused the performance results to be slightly exaggerated. The 18 lbf-sec/lbm difference between the results for this configuration and the other two would have been more like 13 at 100 psia.

The highest performance observed for the stratified flow and 5% BLC injectors was 385 lbf-sec/lbm at mixture ratios of approximately 3.5:1. A value at the nominal mixture ratio of 3.0:1 can be estimated by extrapolation to be 390 lbf-sec/lbm. This compares with 372 for the 10% nominal BLC injector and 408 lbf-sec/lbm for the uniform flow gaseous $B_2H_6$ injector of NASw-1229.

Injector efficiency data for each of the injector configurations are shown in Figs. 4 to 6 and summarized in Fig. 7*. Figs. 8 through 11 contain similar information on thrust chamber efficiency. It is apparent that the difference in specific impulse for the different designs cannot be correlated quantitatively with either injector or thrust chamber efficiency alone. Even trends for the stratified design are noticeably different than for the BLC, while the specific impulse curves are nearly parallel. Thrust chamber efficiency results from NASw-1229 are shown in Fig. 11 for comparison. However, it is significant that while the variations in injector efficiency were over a range of 15 percent, thrust chamber efficiency varied only about 3 percent. A thrust chamber efficiency value of 93 percent could be used for preliminary design studies with any injector efficiency and probably be within 1 percent of the correct value.

## HEAT TRANSFER RESULTS

For graphical convenience the heat flux results are presented separately for the combustor and nozzle. Heat flux instrumentation is described on page 70 and data reduction procedures on page 77. All heat flux data have been modified by the ratio $(100/P_c)^{0.8}$ to correct the results to the nominal test conditions.



*Injector Efficiency is defined on page 74.

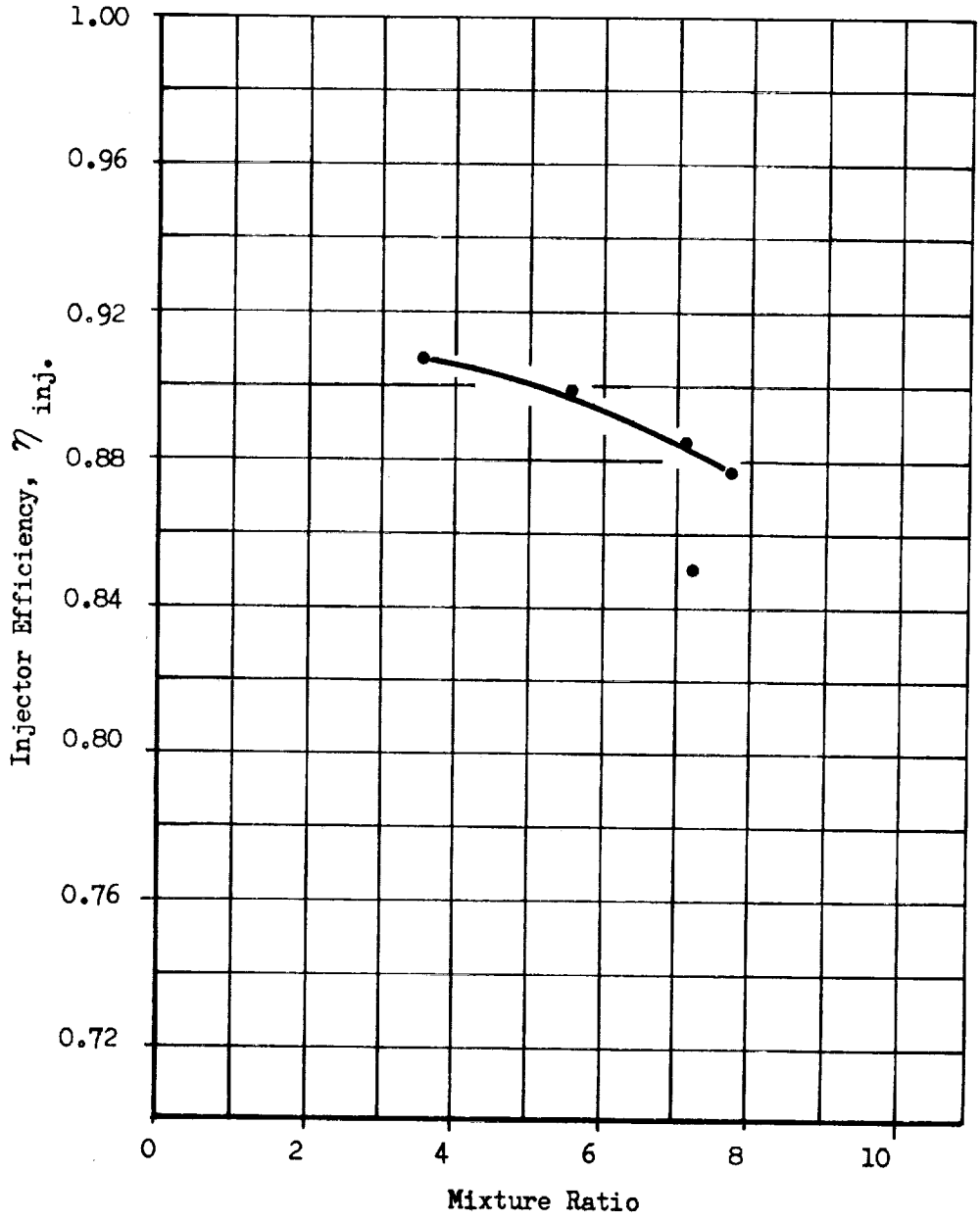


Figure 4 . Injector Efficiency Results for Stratified Test

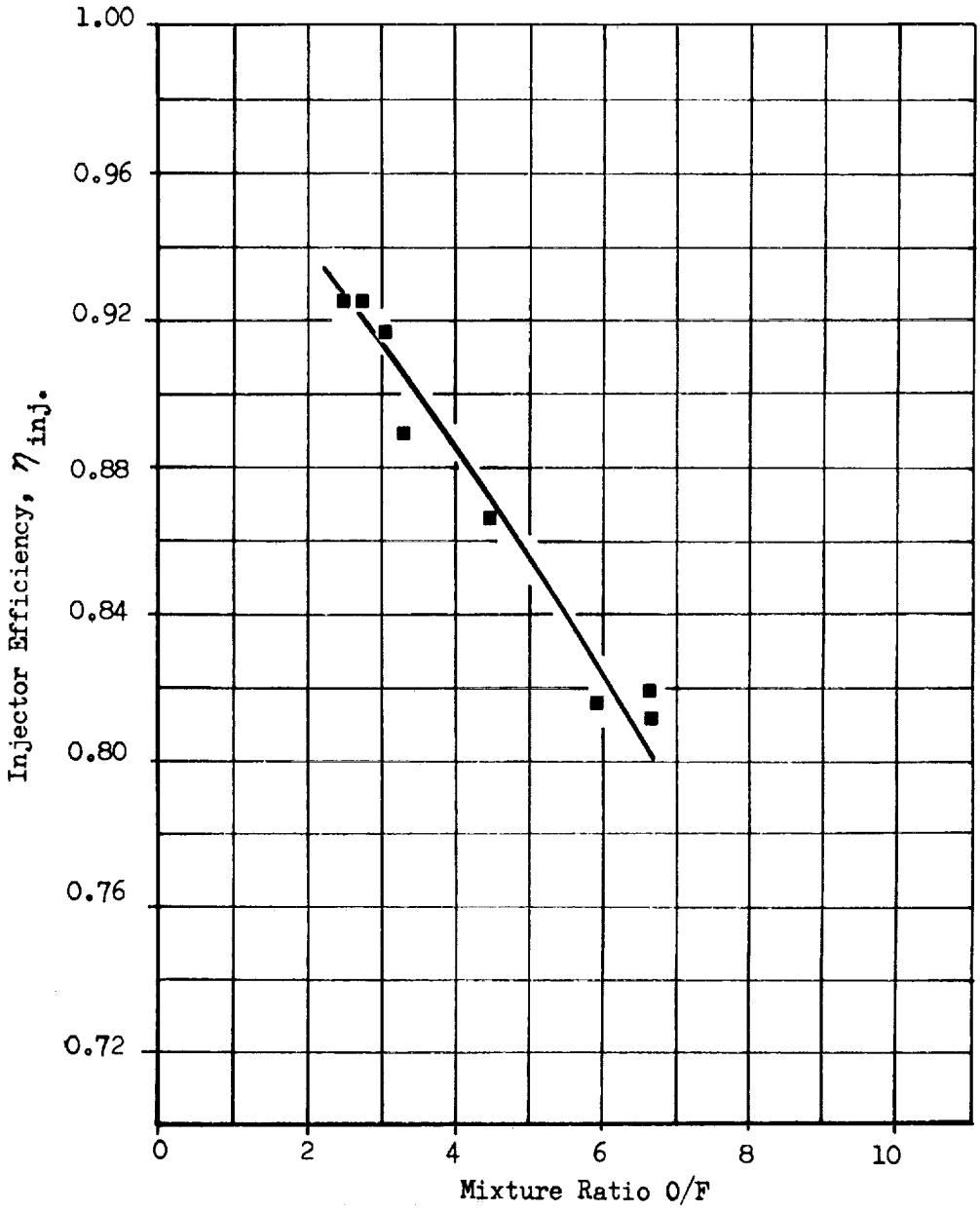


Figure 5. Injector Efficiency Results for 10% BLC Test

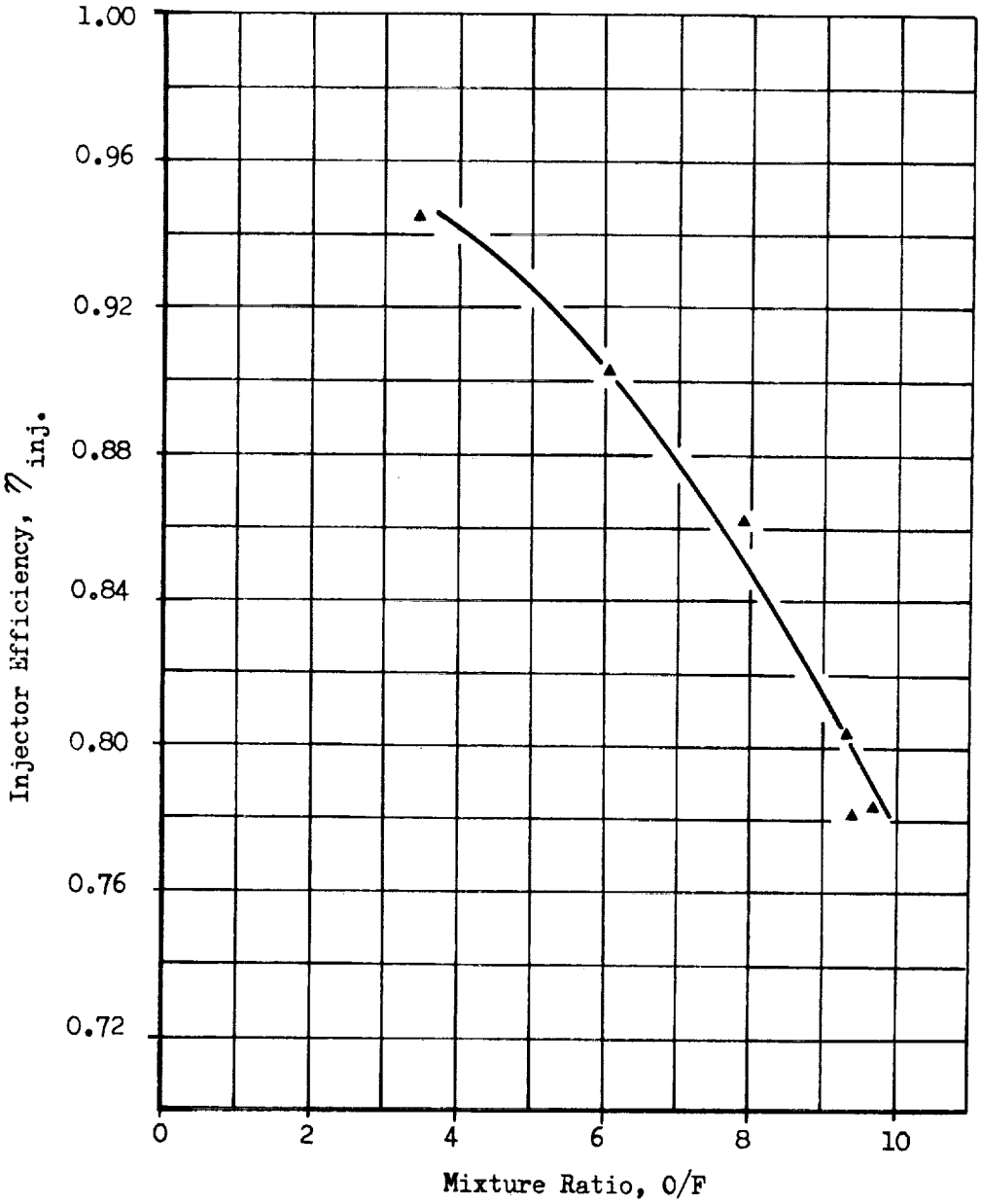


Figure 6 . Injector Efficiency Results for 5% BLC Test

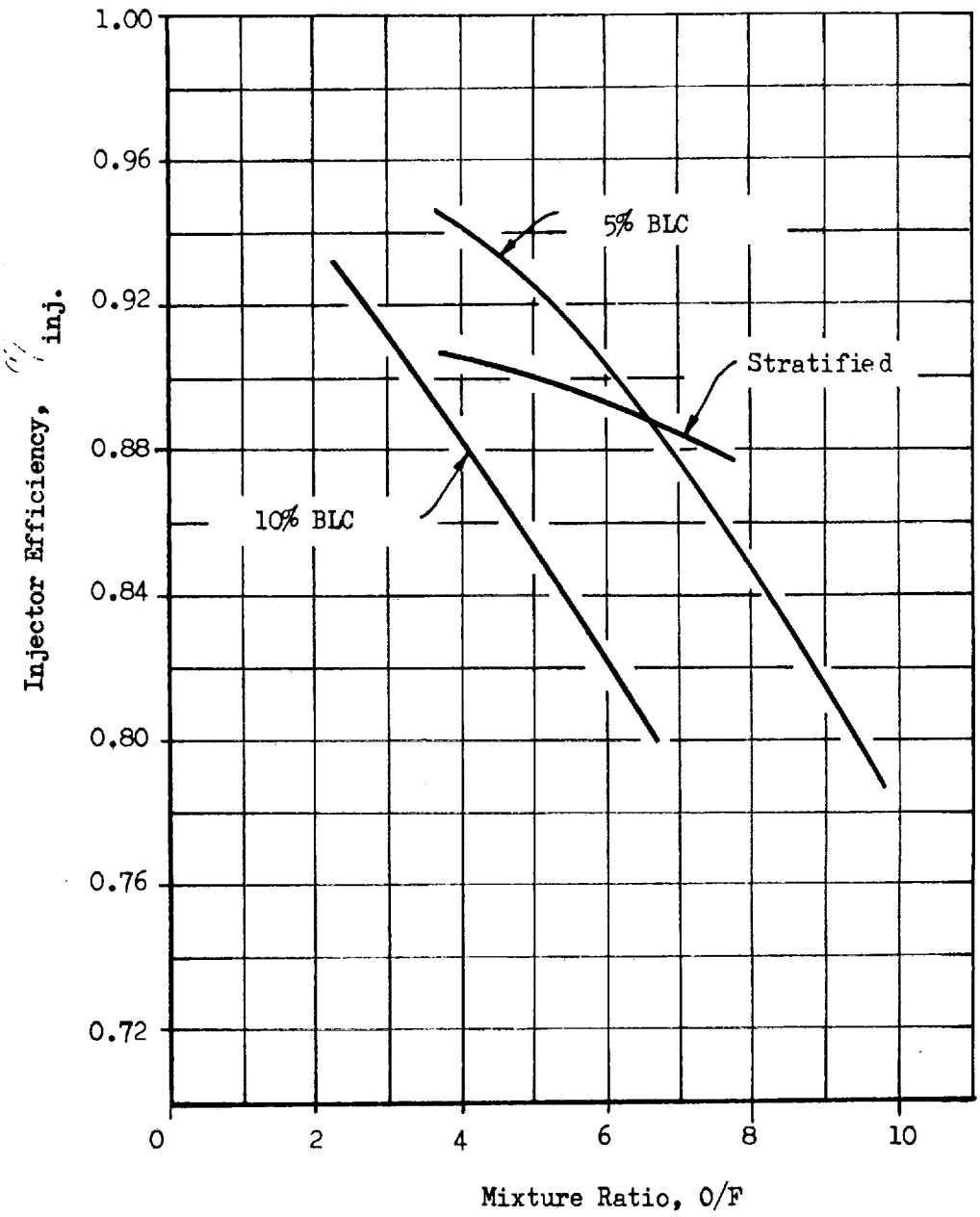


Figure 7. Injector Efficiency Test Results Summary

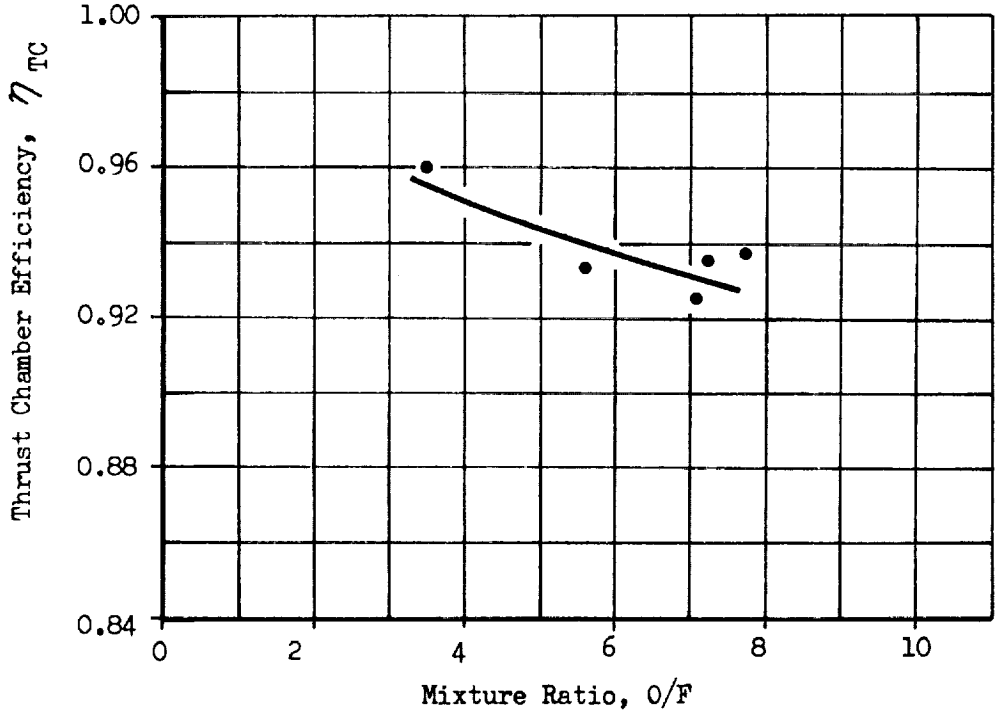


Figure 8. Thrust Chamber Efficiency Results for Stratified Test 073-077

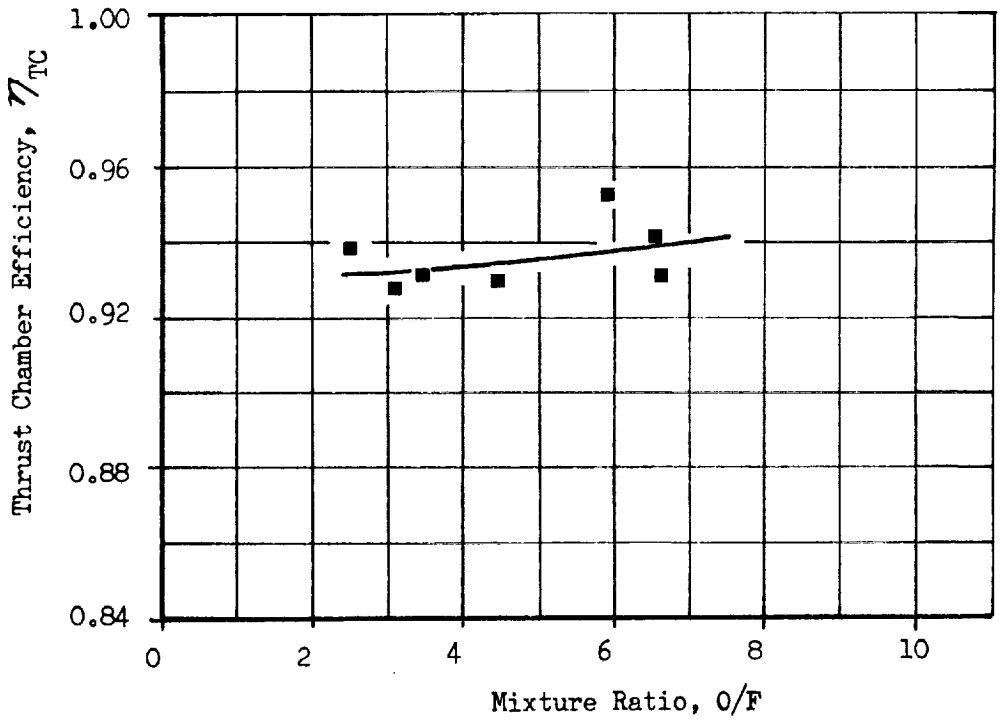


Figure 9. Thrust Chamber Efficiency Results for 10% BLC Test 078-084

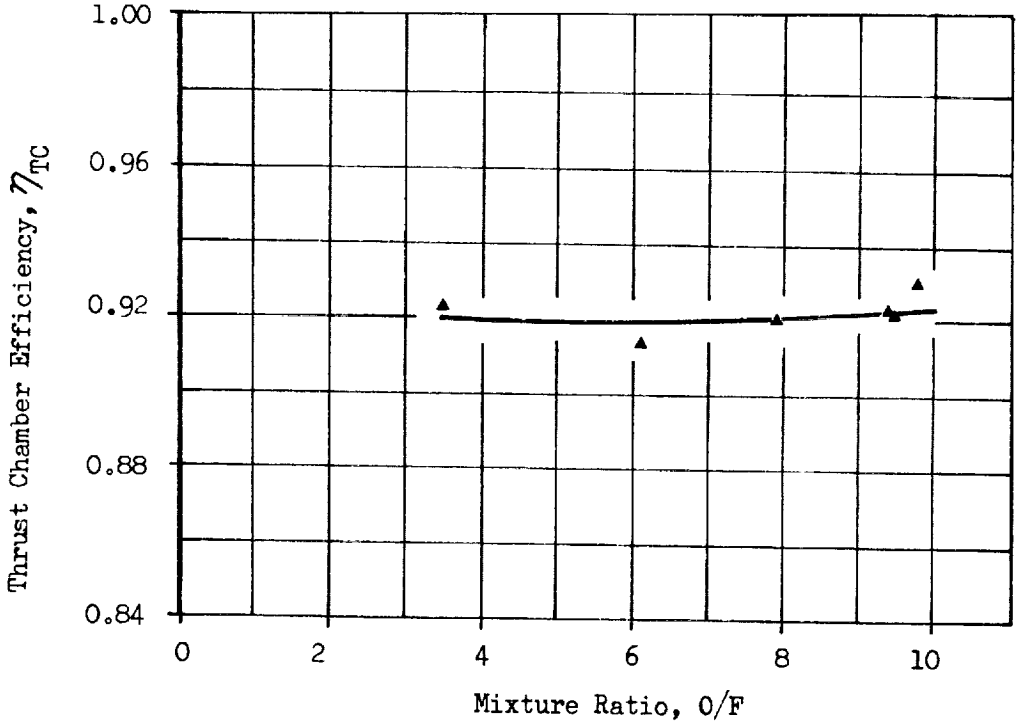


Figure 10. Thrust Chamber Efficiency Results for 5% BLC Test 085-092

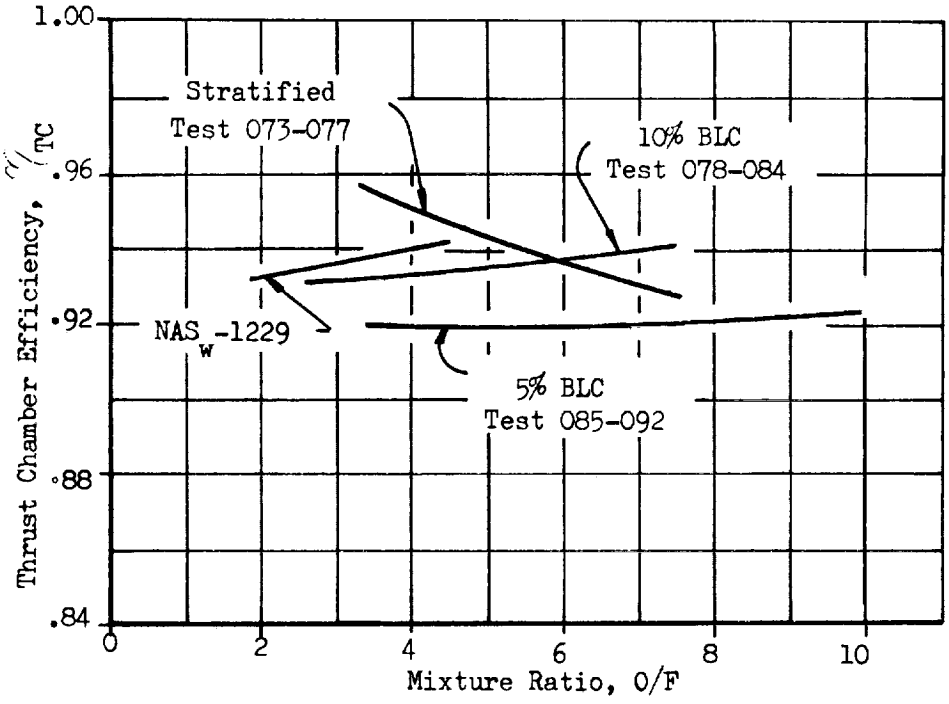


Figure 11. Thrust Chamber Efficiency Test Results Summary

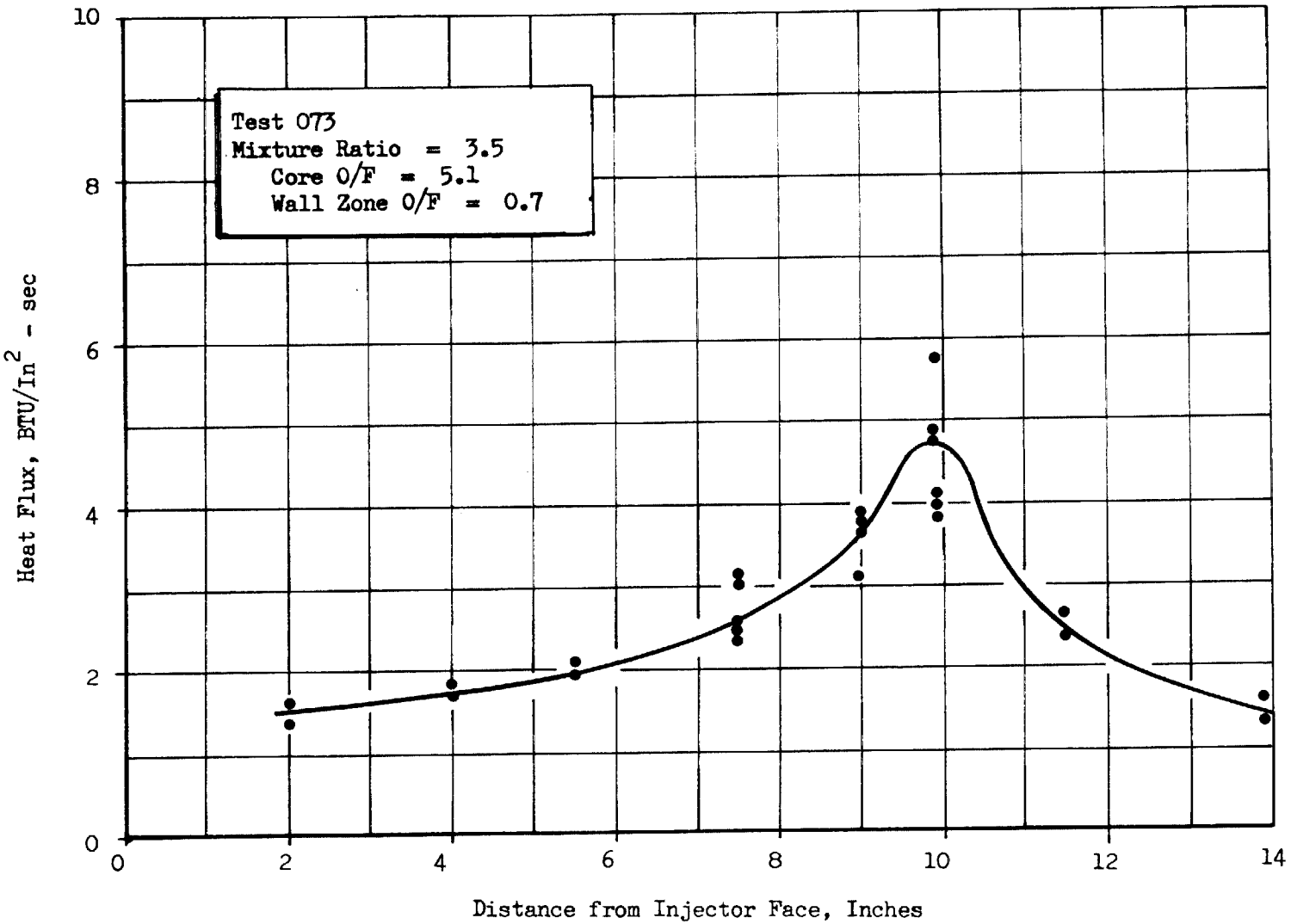


Figure 12. Combustion Chamber Heat Flux Distribution for Stratified Injector

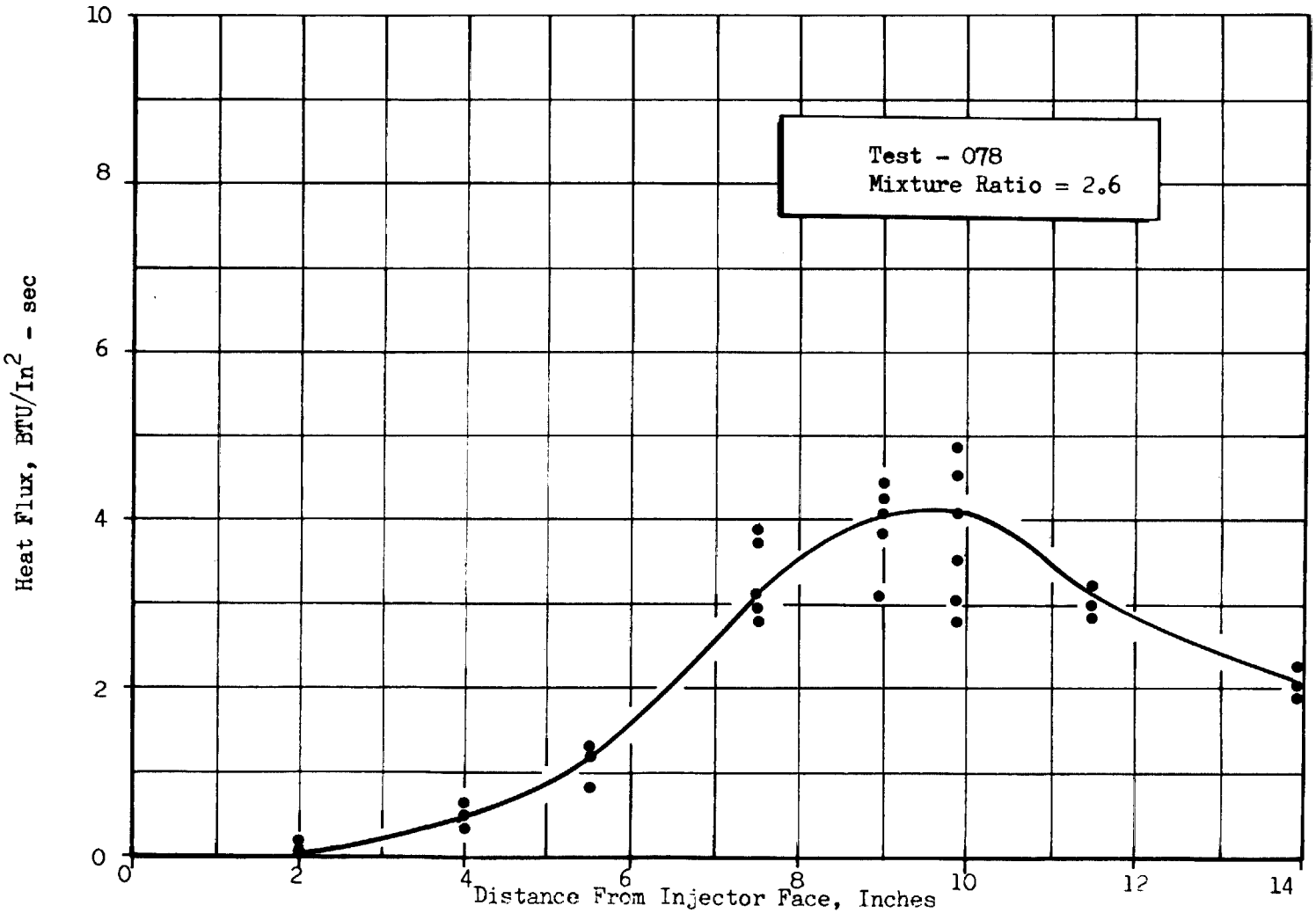


Figure 13. Combustion Chamber Heat Flux Distribution for 10%-BLC Injector

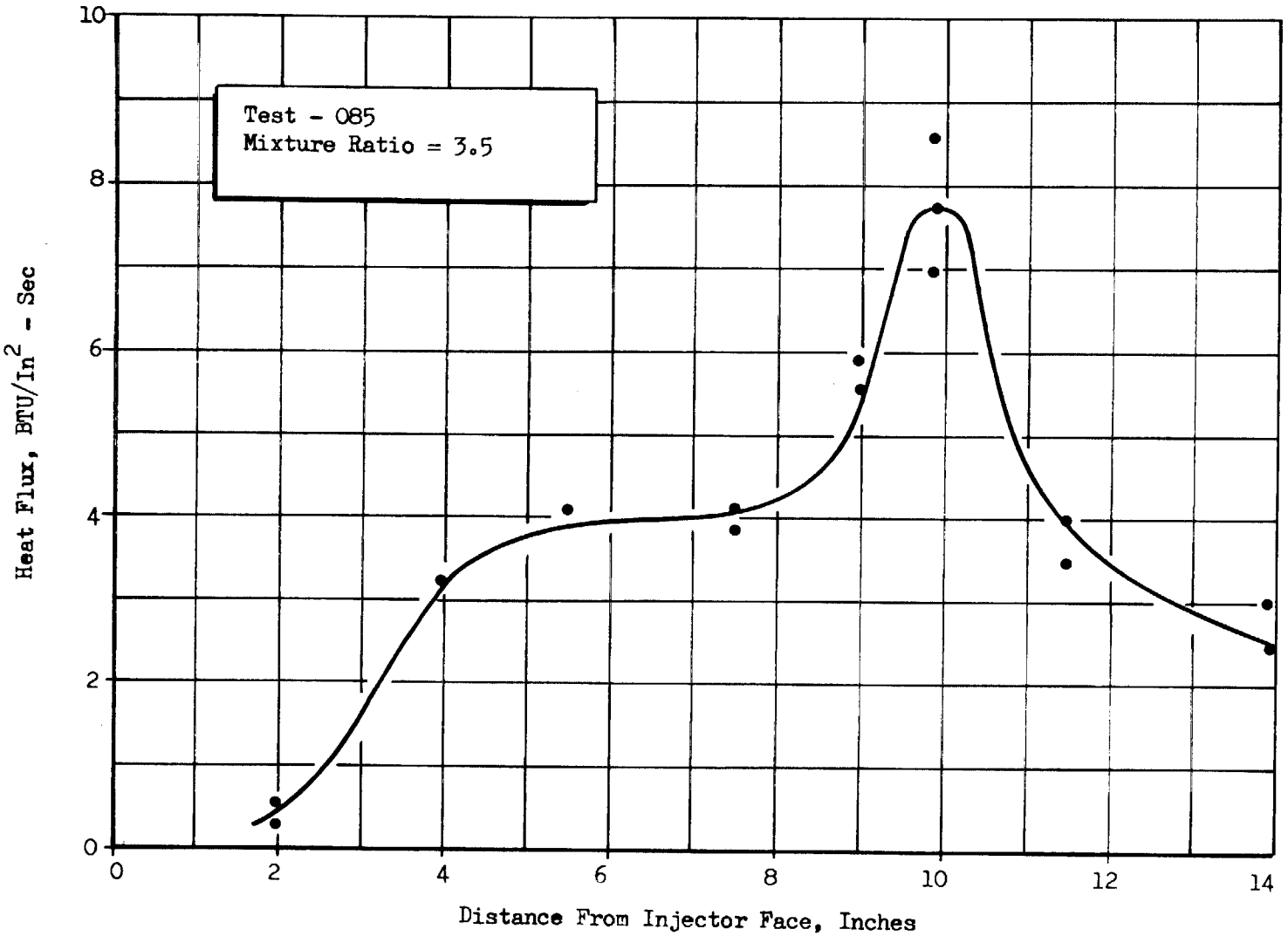


Figure 14 . Combustion Chamber Heat Flux Distribution for 5%-BLC Injector

Combustion Chamber Heat Transfer

Figs. 12 through 14 present combustion chamber heat flux data for each of the injectors. The data are for the lowest mixture ratio test achieved on each injector. Multiple data points indicate multiple data slices and/or multiple thermocouple locations. The solid line indicates the average of the data.

These average lines are superimposed in Fig. 15 for comparison. The heat flux profiles from the unstratified tests on NASw-1229 are also shown. Throat heat flux for the stratified and 10% nominal BLC configurations are seen to be roughly comparable, while the 5% nominal BLC showed no apparent advantage over the unstratified injector. In the combustor zone the 10% BLC produced virtually zero heat flux for the first 3 inches of the combustor. This compares with 1-2 $BTU/In^2$-Sec for the stratified injector. Nozzle heat flux, however, shows the opposite trend. This is covered in more detail in the discussion of nozzle heat transfer.

For further clarity in interpreting the chamber and throat heat flux results the stratified injector data are compared with stratified data from NAS7-304 in Fig. 16 ; and a film cooled data comparison is shown in Fig. 17.

The combustion chamber used with the stratified injectors in NAS7-304 was identical to the one used in this program. Therefore, the comparison is strictly between injector configurations. Figure 16 contains results for four combinations of stratification, 20% and 30% of the total flow in the outer zone and outer zone mixture ratios of 0.5:1 and 1.0:1. The results are ordered as anticipated. Low outer zone mixture ratios and high outer zone flow rates produce low heat flux.

The film cooling results from the two programs are compared in Fig. 17. Here the same injector was used and the variable is combustion chamber length, 5.5 inches for NAS7-304 versus 10.1 inches for this program. For comparable test cases the throat heat flux was 1.5 $BTU/In^2$-Sec for the short chamber versus 4.2 $BTU/In^2$-Sec for the longer chamber. For both chamber lengths, the initial portion of the chamber experienced similar heat flux levels, i.e., the liquid film behaved in a comparable manner.

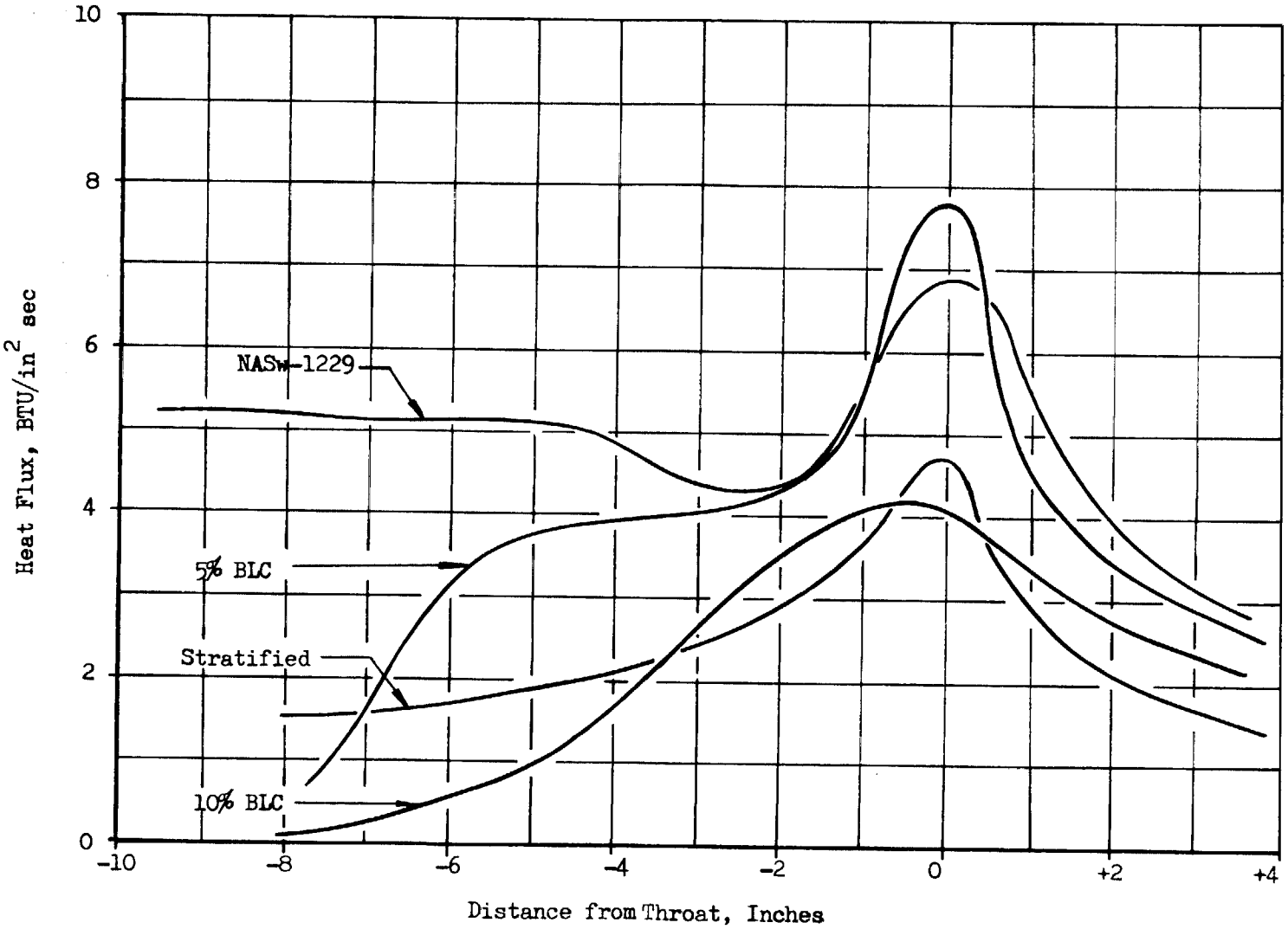


Figure 15. Chamber Heat Flux Comparison

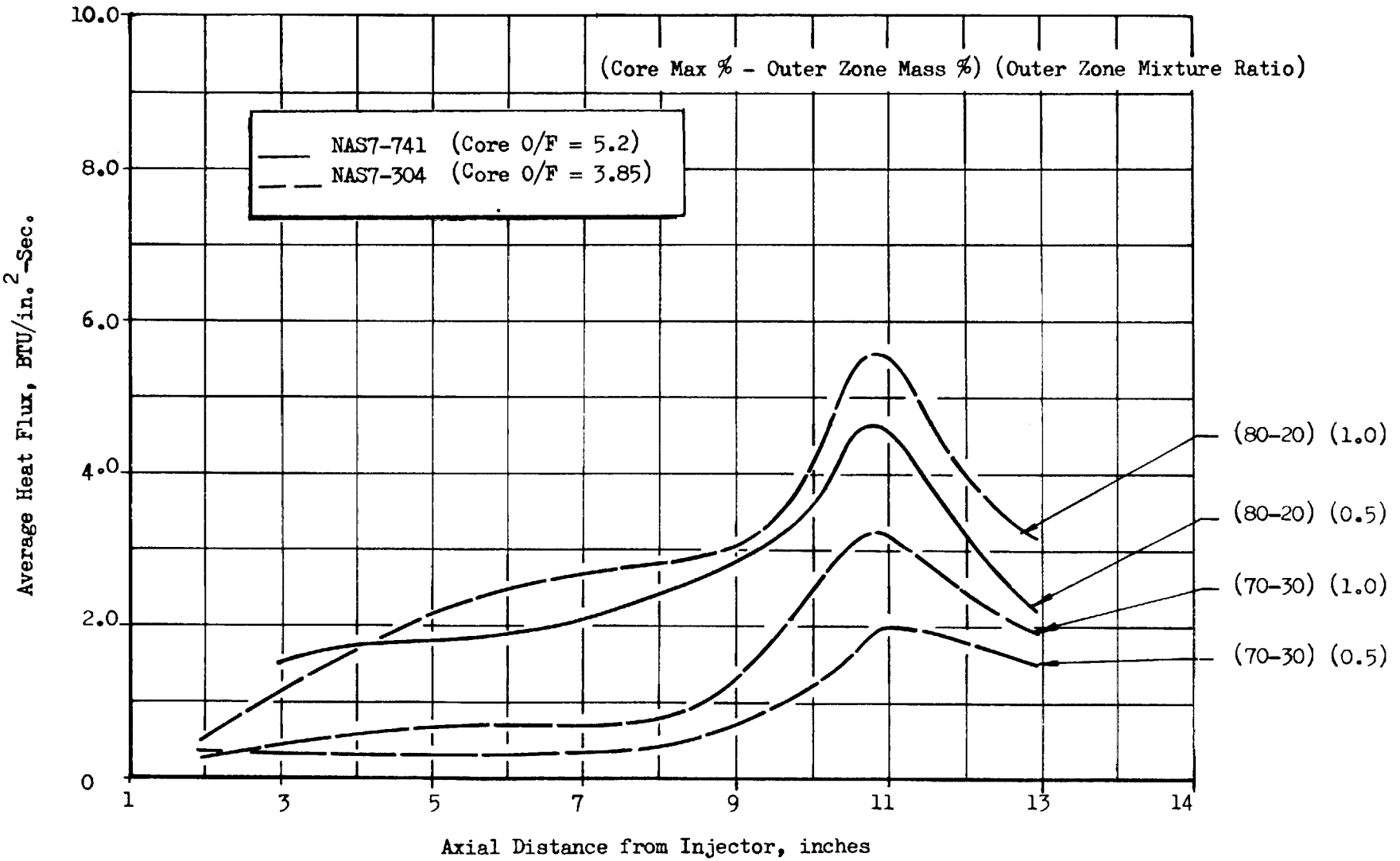


**Figure** 16. Chamber Heat Flux Comparison for Stratified Injectors

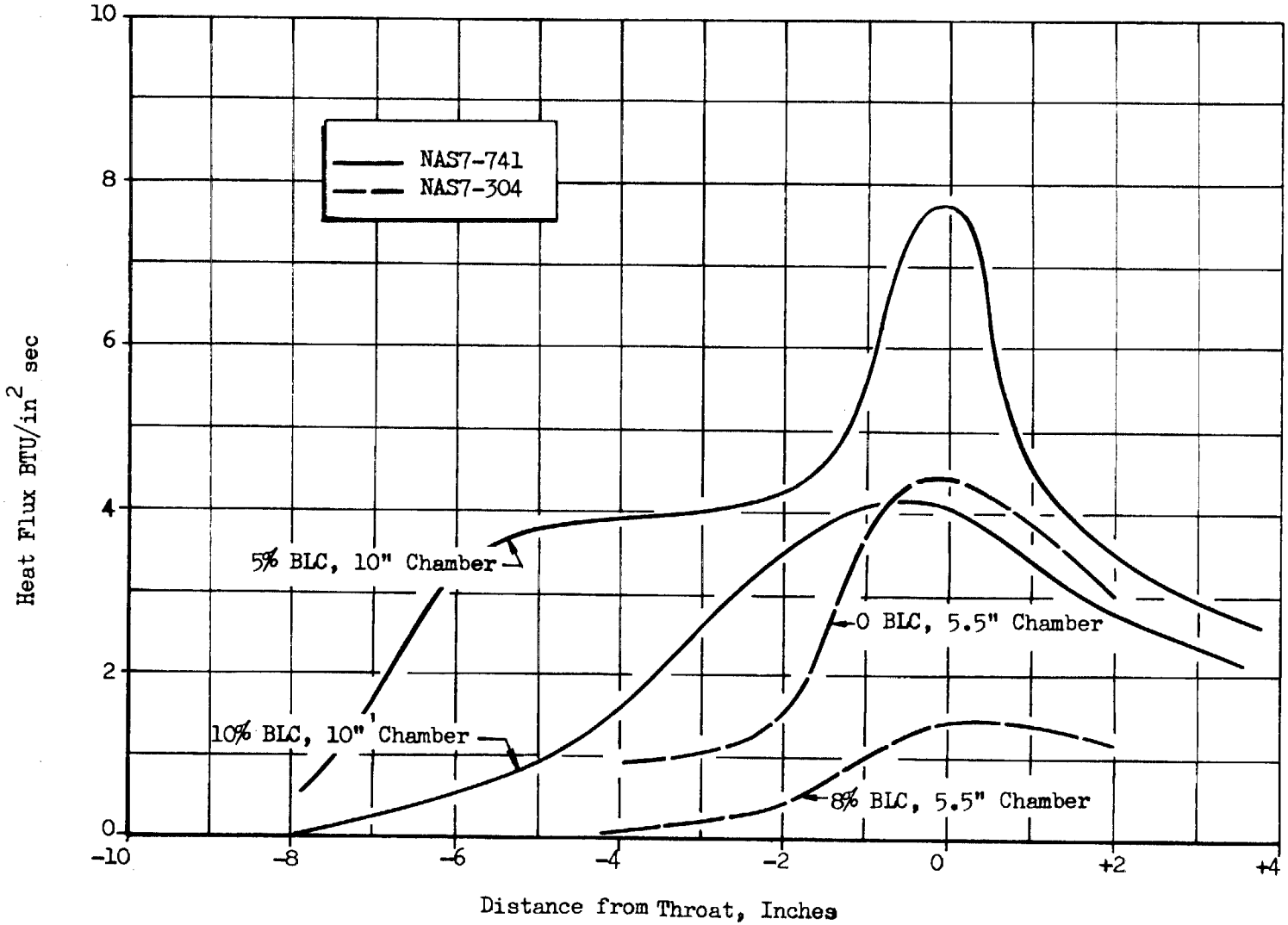


**Figure** 17. Chamber Heat Flux Comparison for BLC Injectors

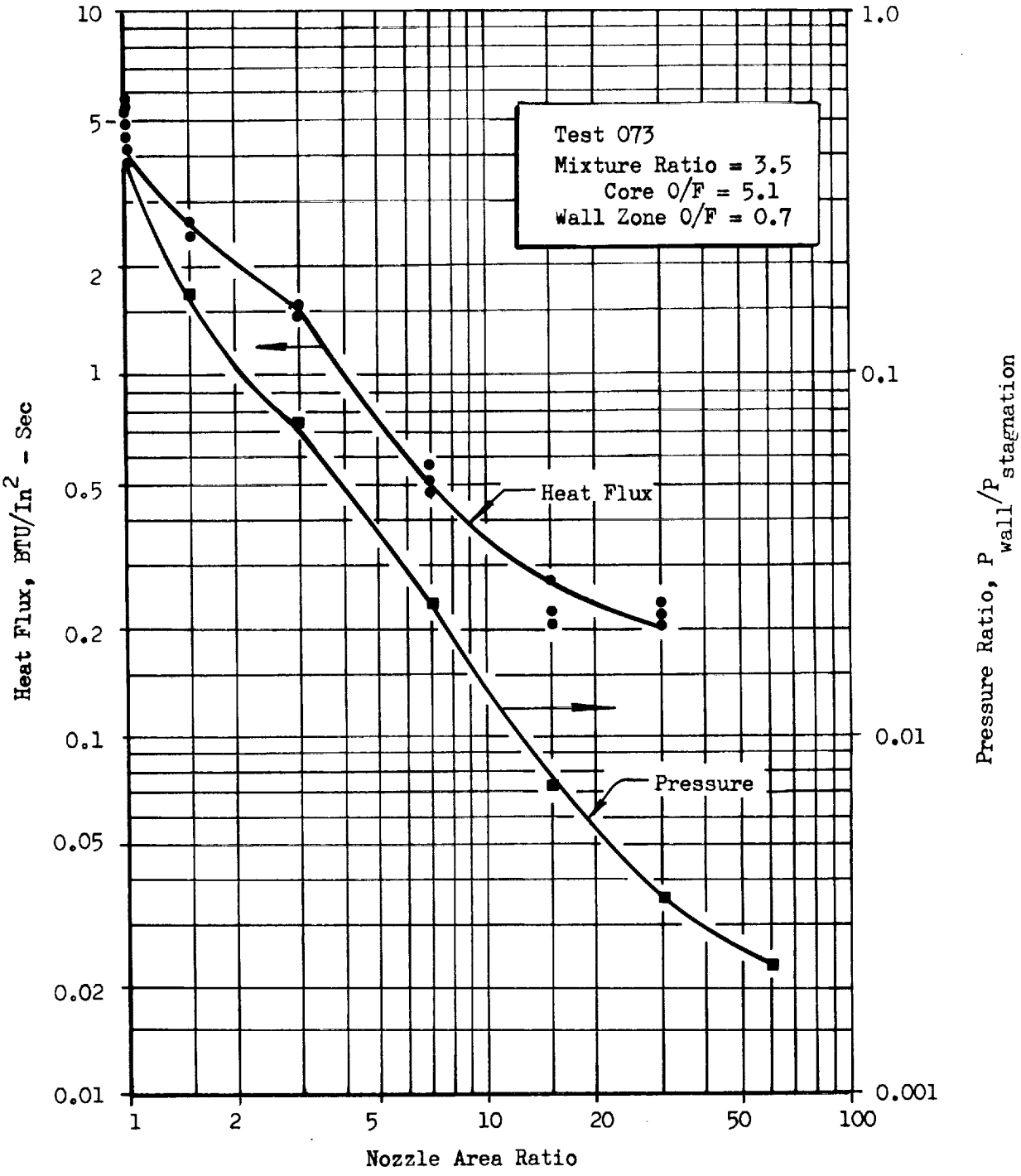


Figure 18. Nozzle Heat Flux and Wall Pressure Profile for Stratified Injector

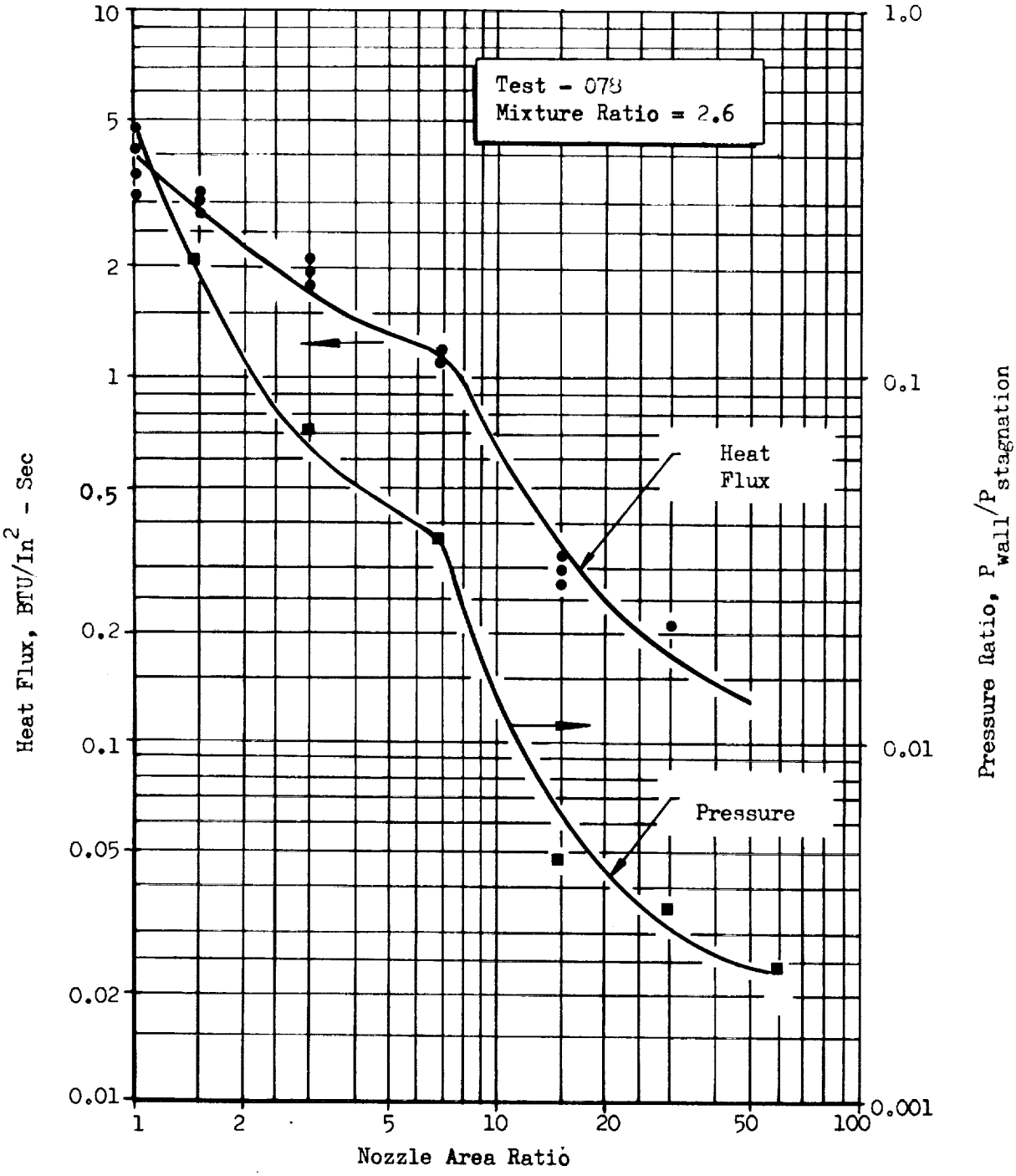


Figure 19. Nozzle Heat Flux and Wall Pressure Profile for 10% Nominal BLC Injector

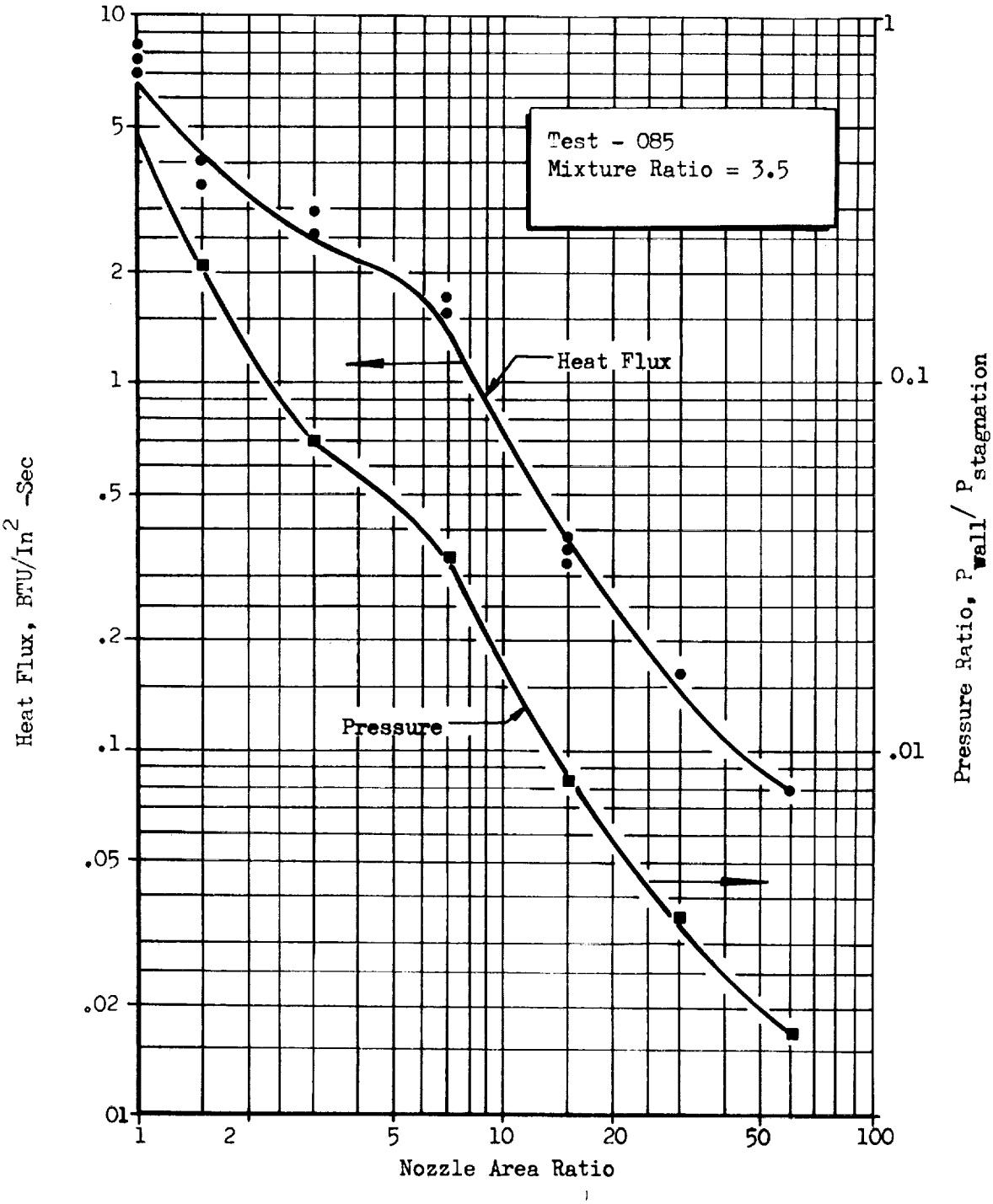


Figure 20. Nozzle Heat Flux and Wall Pressure Profile for 5% Nominal BLC Injector

Nozzle Heat Transfer Results

Nozzle heat flux results are presented in Fig.18 through 20 for the three injector configurations. Because of an unusual trend in the heat flux profiles, the wall pressure profiles are also shown. In each case the results show high heat flux and wall pressure in the vicinity of area ratios 3:1-7:1 and a general upward curvature in the high area ratio portion of the nozzle. This behavior would not be expected from one dimensional isentropic expansion analysis. However, the method of characteristics does predict this trend as shown in Fig. 21, although not as dramatically as seen in the data. The phenomenon results from reflection of characteristic waves from the nozzle wall off the centerline. The disturbance initiates in the circular region at the throat. Fig. 22 is reproduced from Ref. 4 and demonstrates the effect of this phenomenon on the geometric efficiency as a function of area ratio. The same result has been reported in Ref. 5.

The heat flux profiles from all three injectors are shown in Fig. 23 together with the results for the unstratified injector in NASw-1229. At the low area ratios, the region of primary concern, the stratified injector produced lower heat flux than the 10% BLC by an amount which varied up to a maximum of 50% at an area ratio of about 7:1. This result is probably due to the rate of mixing between the protective layer of gas and the adjacent portion of the core. If, for example, the 10% film mixed with the gas from the outer row of doublets the resulting flow would constitute 37% of the total mass at a mixture ratio of 1.3. This contrasts with injected values for the stratified injector of 20% at a mixture ratio of 0.5:1, and would be expected to produce higher heat flux. In the chamber, however, before mixing occurs the film cooled injector provides better protection, as was seen in Fig. 15. For shorter combustion chambers this effect would be expected to be delayed until further into the nozzle where it would be less important.

The 5% BLC injector shows very high heat flux. The NASw-1229 results are also shown and indicate that both the stratified and 10% BLC injectors provide protection during at least part of the nozzle, the stratified protection lasting considerably longer.

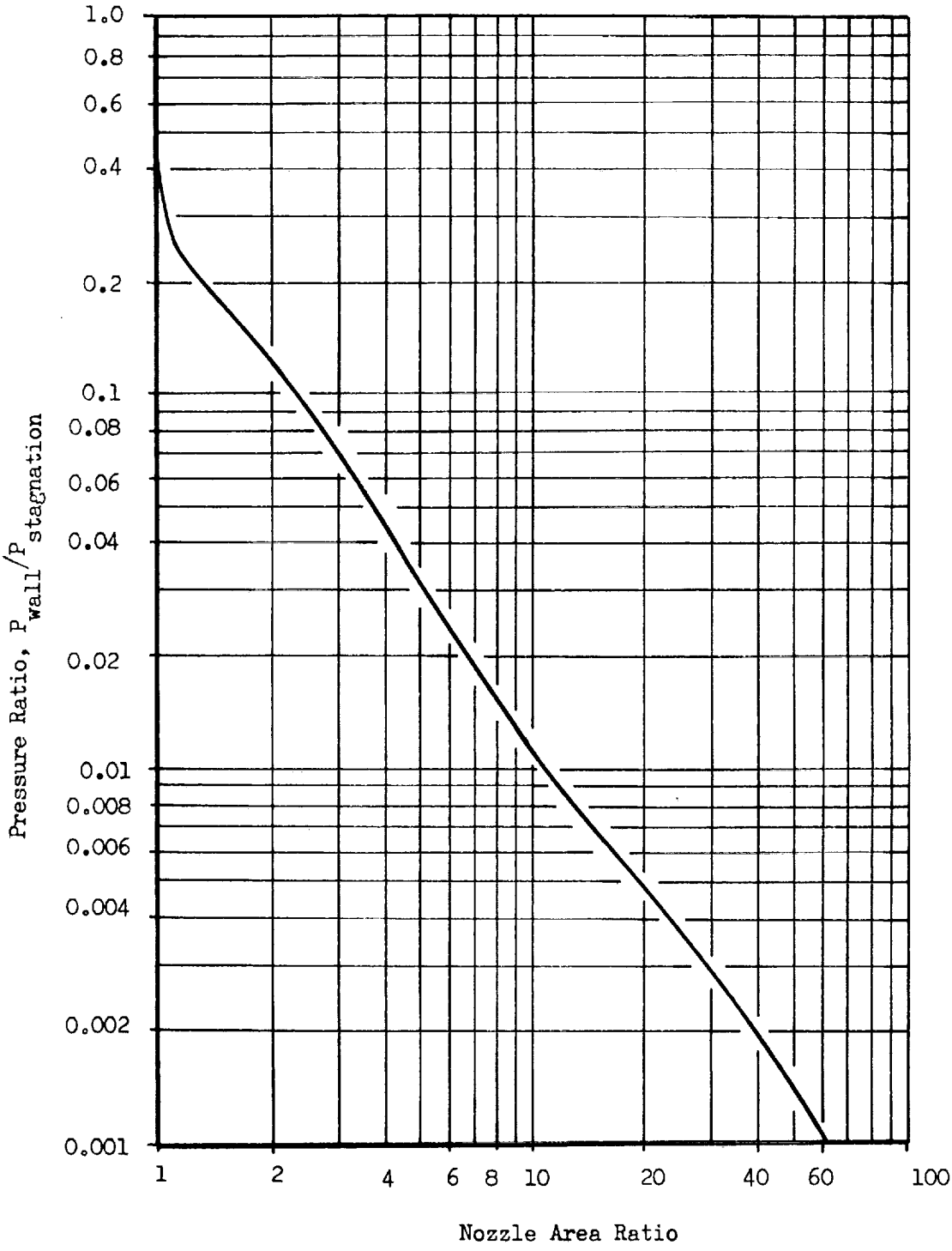


Figure 21. Predicted Wall Pressure Profile for 15-degree Conical Nozzle

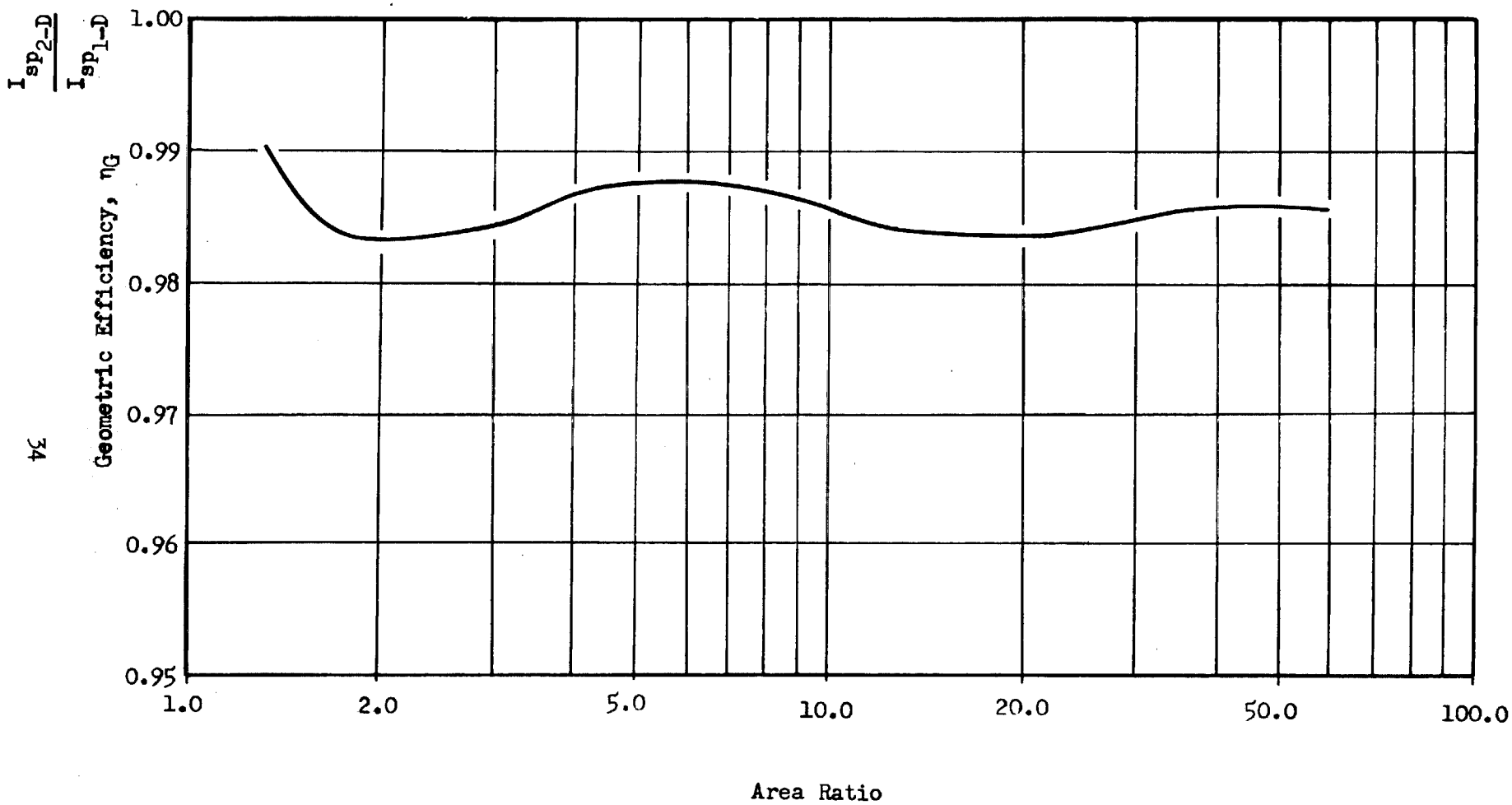


**Figure 22.** Effect of Area Ratio on Geometric Efficiency of a 15-Degree Conical Nozzle

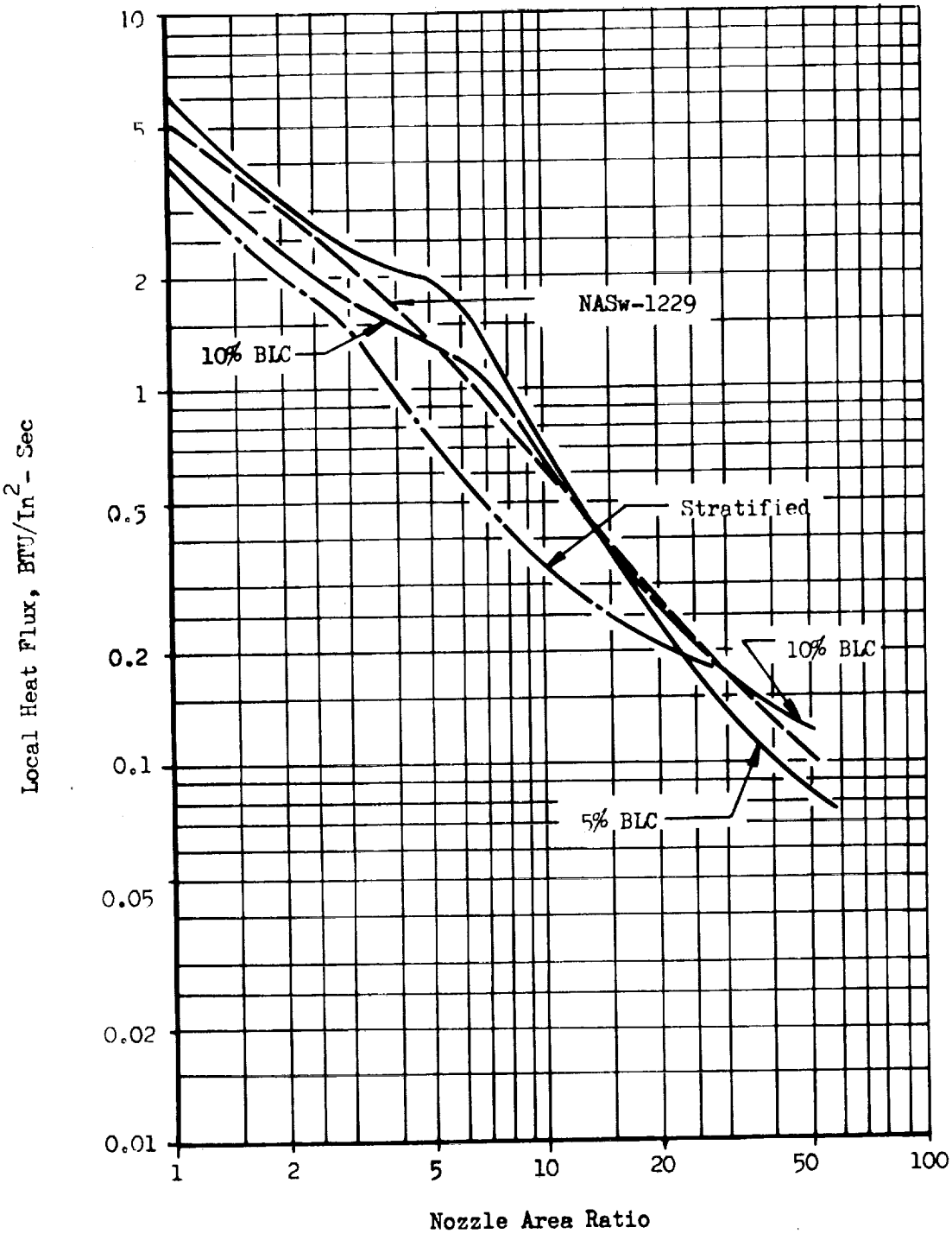


**Figure 23.** Nozzle Heat Flux Comparison

## DIBORANE FLOW BLOCKAGE

Throughout this test program, the diborane injector pressure drop was approximately 5-10 times the value indicated by the freon calibration data. The same was not true of the oxygen difluoride, which reproduced the calibration pressure drops for the oxidizer side of the injector. The film cooled injector, which had been fired previously in NAS7-304 also produced very high diborane pressure drops in this program. The only significant difference between the two test programs was the diborane temperature. In this program the diborane was fed to the engine at approximately -200°F, over 100 degrees colder than used in NAS7-304.

The blockage occurred in two different injectors and for initial injector temperatures from 0°F down to -150°F. The oxidizer was introduced at the same temperature as the fuel and could not have induced freezing.

A satisfactory explanation does not exist at this time but the consistency with which the phenomenon occurred indicates that this is a problem requiring further investigation.

## COMBUSTION PRODUCT DEPOSITION

Because the stratified injector used in this program was similar to those used in NAS7-304 and the BLC injector was the same one used in that program, deposition results were expected to be the same. The results were not the same, but because the test program was very limited in scope, the cause was not isolated and remains an unanswered question. However, the extreme mixture ratios tested are presumed to be the most likely cause.

The stratified flow injector deposit was greater than NAS7-304 observed for similar injectors but not unusual in appearance.

The BLC injector developed a long protruding deposit during the 5% BLC test series. This deposit, shown in Fig. 24, was gravitationally oriented, as though it were flowing slowly out of the injector and chamber. The test data do not indicate the cause of this type of deposit.

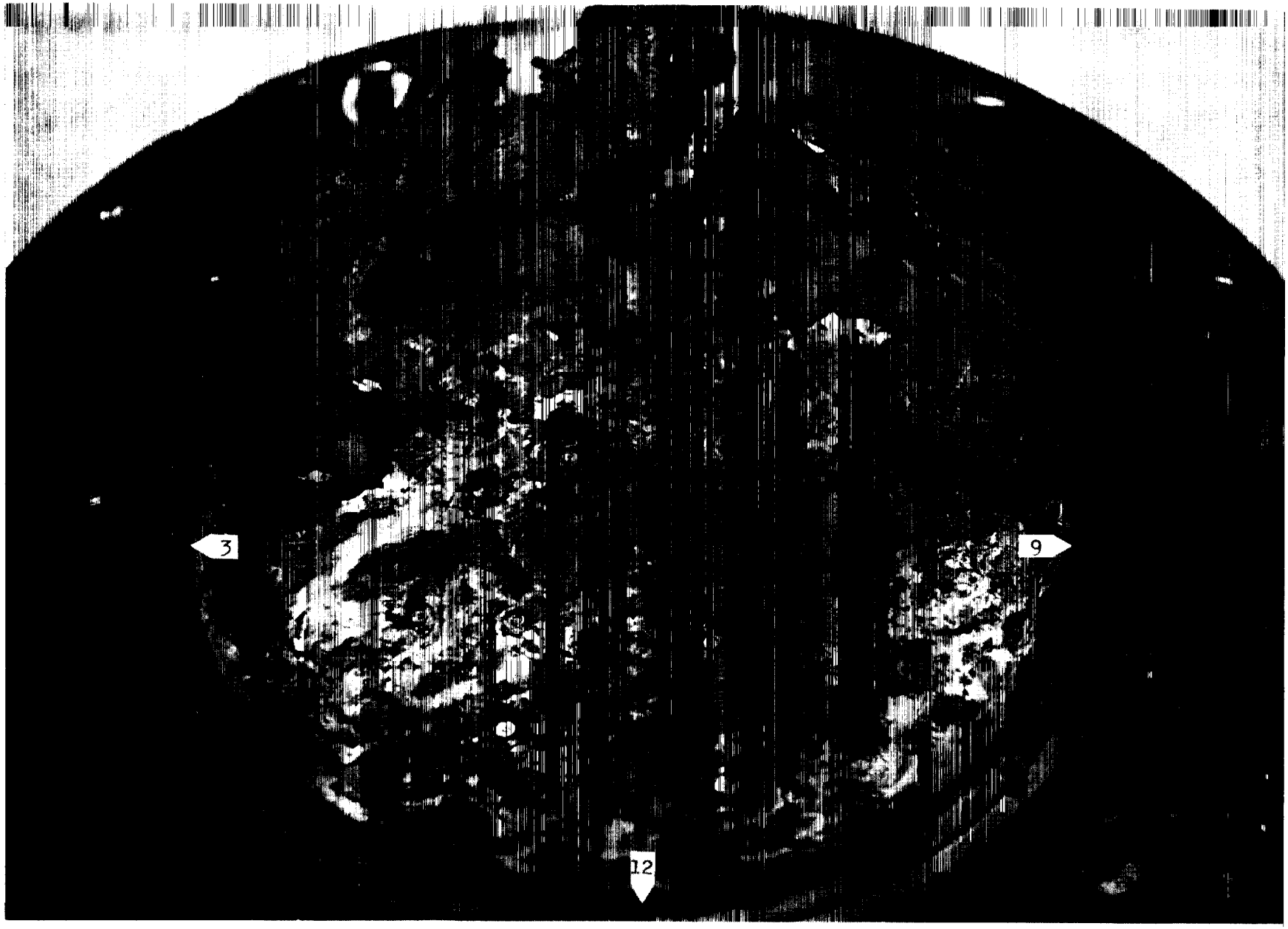


1XW45-10/30/69-R1C

Figure 24. Injector Deposits, 5% BLC Test Series

## TEST HARDWARE

New rocket engine hardware fabricated for this program consisted of a mixture ratio stratified injector, a combustion chamber, and a high area ratio conical nozzle. A film cooled injector was damaged during the final steps of fabrication and was replaced by the film cooled injector originally used in another $OF_2/B_2H_6$ project, NAS7-304. The hardware was designed for a nominal vacuum thrust of 1000 pounds and a chamber pressure of 100 psia. Heavy wall, heat sink designs were used.

### INJECTORS

Details of the three injectors are summarized in Table 2 and 3. The first table contains information describing the injector geometry, while the second concerns design of the injector elements.

#### Stratified Injector

The stratified injector was designed to protect the thrust chamber by placing a barrier of relatively cool, low mixture ratio combustion products along the combustor wall. Previous results from NAS7-304 indicated that 20-percent of the total propellant flowrate at a mixture ratio of 0.5:1 would provide adequate combustor protection. The nominal core mixture ratio was set at 3.85:1 to provide maximum performance. Nominal overall mixture ratio was thus 2.36:1. Core mixture ratio, outer zone mixture ratio, and percent of total mass in the outer zone are shown as a function of overall mixture ratio in Fig. 25.

The injector element arrangement consists essentially of 3 rows of like-on-like doublet elements, 40 for the oxidizer and 50 for the fuel. Details of the injector are shown in Fig. 26, which indicates the element pattern and propellant manifolding, and Table 3 which tabulates critical dimensions of the injector elements. A photograph of the completed injector is shown in Fig. 27. The outer row was designed with the fuel elements offset toward the wall from the oxidizer elements, providing some additional protection.

TABLE 2

INJECTOR DESIGN DETAILS

| ITEM | STRATIFIED | BLC SWIRL |
|---|---|---|
| Basic | | |
| Chamber Pressure, psia | 100 | 100 |
| Throat Diameter, in. | 2.54 | 2.54 |
| Chamber Diameter, in. | 3.72 | 3.72 |
| Contraction Ratio | 2.14 | 2.14 |
| Impingement Angle Included, degrees | 60 | 60 |
| Mixture Ratio | | |
| Overall | 2.36 | 2.40 |
| Inner Ring | 3.85 | 3.85 |
| Middle Ring | 3.85 | 3.85 |
| Outer Ring | 0.50 | 3.20 |
| Mass Flow Percent | | |
| Inner Ring | 26.7 | 21.0 |
| Middle Ring | 53.3 | 42.0 |
| Outer Ring | 20.0 | 27.0 |
| BLC | - | 10.0 |
| Impingement Diameter, in. | | |
| Inner Ring | 1.360 | 1.220 |
| Middle Ring | 2.720 | 2.120 |
| Outer Ring | | |
| Fuel | 3.500 | 3.130 |
| Ox | 3.110 | 2.788 |

TABLE 3

INJECTOR ELEMENT SPECIFICATION

| Injector Type | Row Location | Number Orifices | Orifice Diameter | Impingement Diameters | Free Stream L/D | Orifice L/D |
|---|---|---|---|---|---|---|
| Stratified | Inner | | | | | |
| | fuel | 20 | 0.0143 | 0.075 | 6.06 | 10.40 |
| | ox | 20 | 0.0273 | 0.140 | 5.92 | 10.15 |
| | Middle | | | | | |
| | fuel | 40 | 0.0143 | 0.075 | 6.06 | 11.84 |
| | ox | 40 | 0.0273 | 0.140 | 5.92 | 10.15 |
| | Outer | | | | | |
| | fuel | 40 | 0.0179 | 0.090 | 5.80 | 10.12 |
| | ox | 20 | 0.0141 | 0.075 | 6.14 | 10.07 |
| Design BLC | Inner | | | | | |
| | Fuel | 20 | 0.0151 | 0.0743 | 5.68 | 10.64 |
| | ox | 20 | 0.0237 | 0.121 | 5.90 | 10.00 |
| | Middle | | | | | |
| | Fuel | 40 | 0.0151 | 0.0743 | 5.68 | 11.85 |
| | ox | 40 | 0.0237 | 0.121 | 5.90 | 10.00 |
| | Outer | | | | | |
| | Fuel | 40 | 0.0137 | 0.0675 | 5.69 | 14.56 |
| | ox | 40 | 0.0198 | 0.101 | 5.88 | 10.02 |
| | BLC | | | | | |
| | Fuel | 16 | 0.025 | | | |
| NAS7-304 BLC | Inner | | | | | |
| | Fuel | 10 | 0.024 | 0.078 | 3.74 | 6.50 |
| | ox | 10 | 0.036 | 0.121 | 3.89 | 6.57 |
| | Middle | | | | | |
| | Fuel | 20 | 0.024 | 0.078 | 3.74 | 6.50 |
| | ox | 20 | 0.036 | 0.121 | 3.89 | 6.57 |
| | Outer | | | | | |
| | Fuel | 40 | 0.0145 | 0.0692 | 5.52 | 10.75 |
| | ox | 40 | 0.020 | 0.091 | 5.25 | 9.45 |
| | BLC | | | | | |
| | Fuel | 16 | 0.020 | Swirl | | |

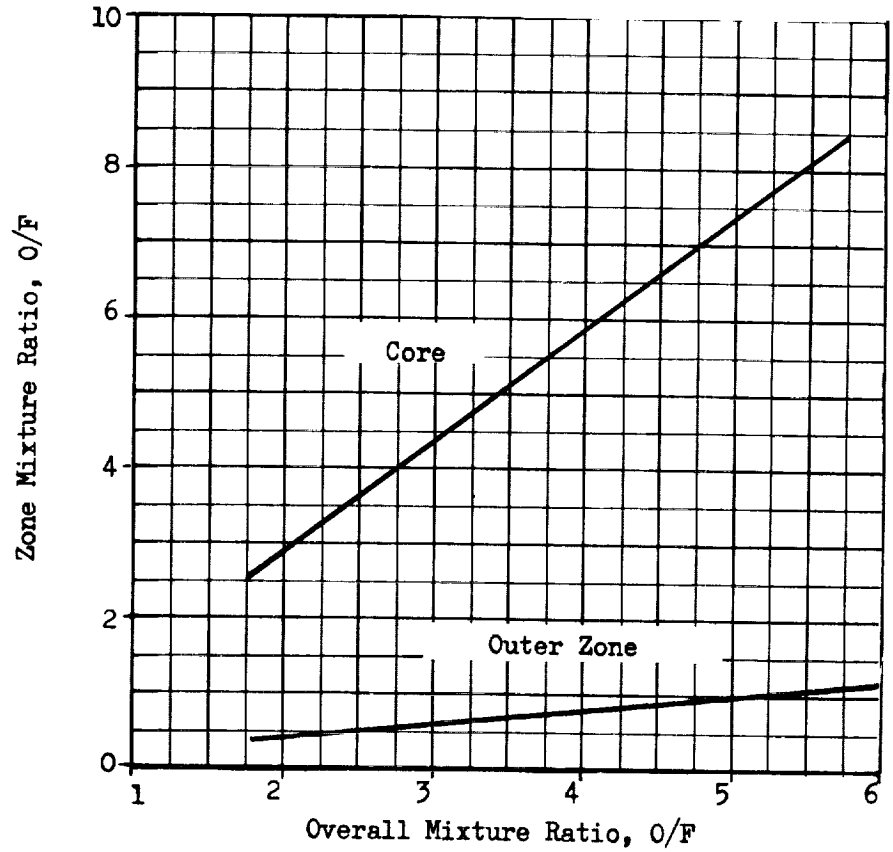


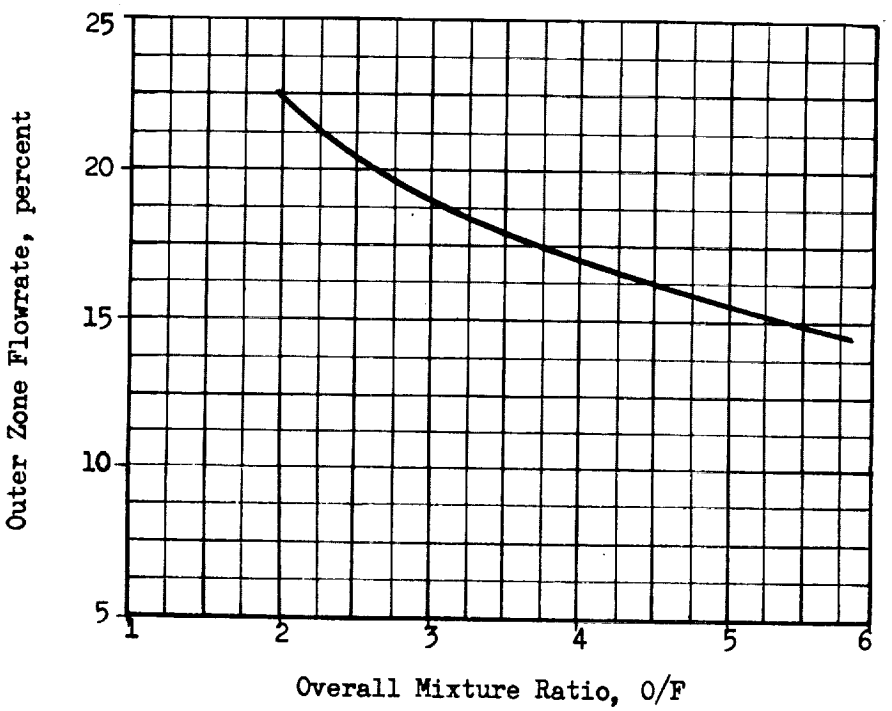


Figure 25. Flow Distribution for Stratified Injector

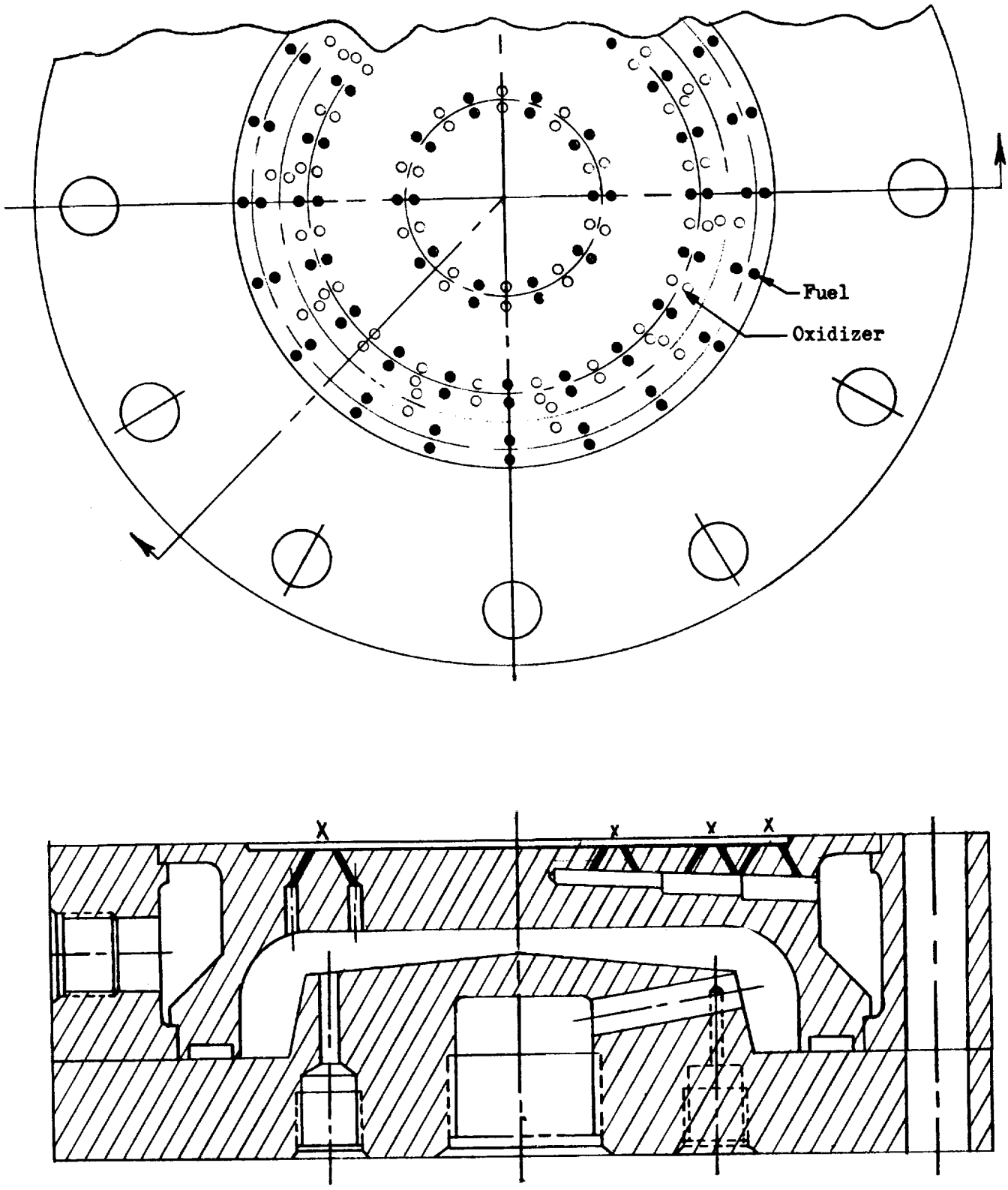


Figure 26. Stratified Injector Design

LXX45-3/6-70-R1A

Figure 27. Stratified Flow Injector Photograph

The injector was of heavy duty design, fabricated in two parts. The core was fabricated using dense nickel 270 to provide critical propellant isolation. Nickel 200 was used to fabricate the manifold ring. The individual parts were subsequently electron beam welded to form an injector assembly. The oxidizer orifice location in the outer row was dictated by the method used for manifolding the injector orifices. Instrumentation on the injector included manifold pressures and temperatures.

Film Cooled Injector

The film cooled injector was designed to use a combination of tangentially swirled liquid film and moderate mixture ratio stratification to provide wall protection. Details of this injector were based on data previously obtained in NAS7-304 with a similar film cooled design. Although this injector was not completed as a result of a manufacturing error, the design details are presented here for reference. The element arrangement is shown in Fig. 28 and element details in Table 3. The injector design is a like-on-like doublet 100 element configuration with tangential film coolant injection.

Film coolant comprises 10-percent of total propellant flow at nominal conditions. Of the 90-percent in the core, the inner two rows use 70-percent at mixture ratio 3.85:1 and the third row uses a 30-percent at mixture ratio 3.2:1. Nominal overall mixture ratio was thus 2.4:1.

NAS7-304 Film Cooled Injector

The film cooled injector used in the test program had been tested previously in Contract NAS7-304. The mass distribution is the same as was planned for the new film cooled injector. It differs only in number of elements (70 vs 100) and degree of symmetry. This injector is described in Figs. 29 and 30 and Table 3. This injector, and the planned new injector were designed for separate control of film coolant flowrate. Tests were conducted with both the nominal value of 10% when average core mixture was 3.85:1 and half

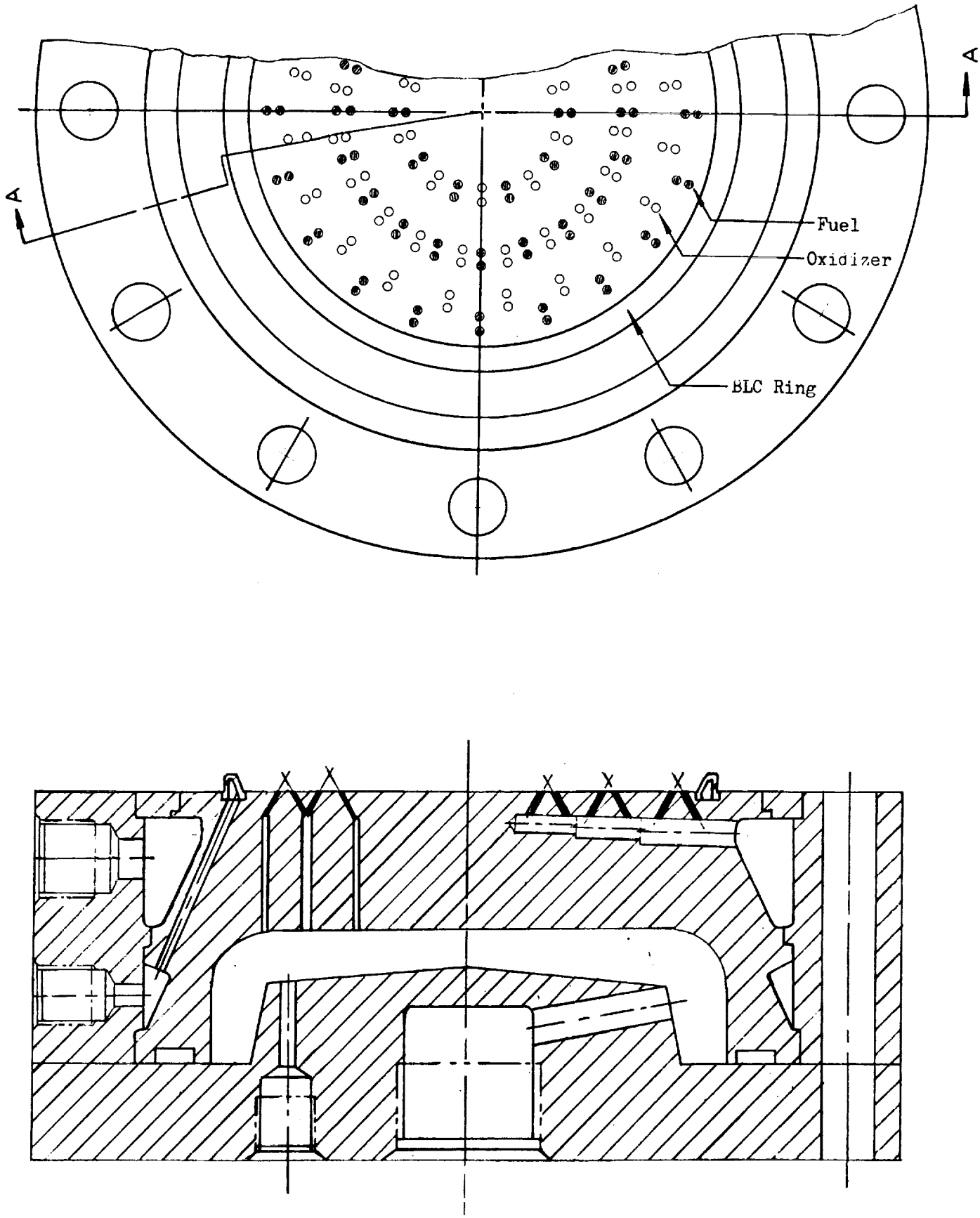


Figure 28. BLC Swirl Injector Design

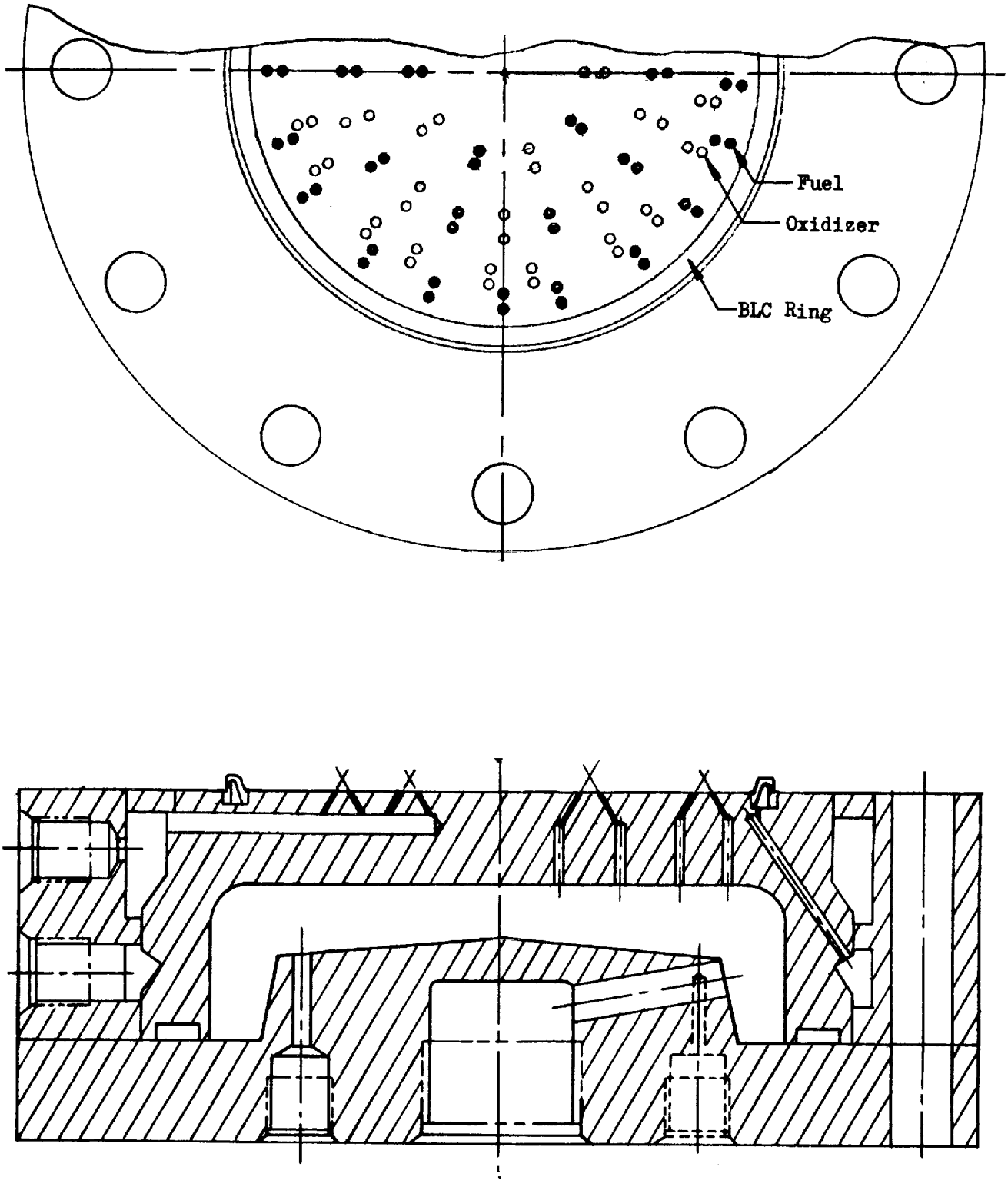


Figure 29. NAS7-304 Boundary Layer Control Injector Design

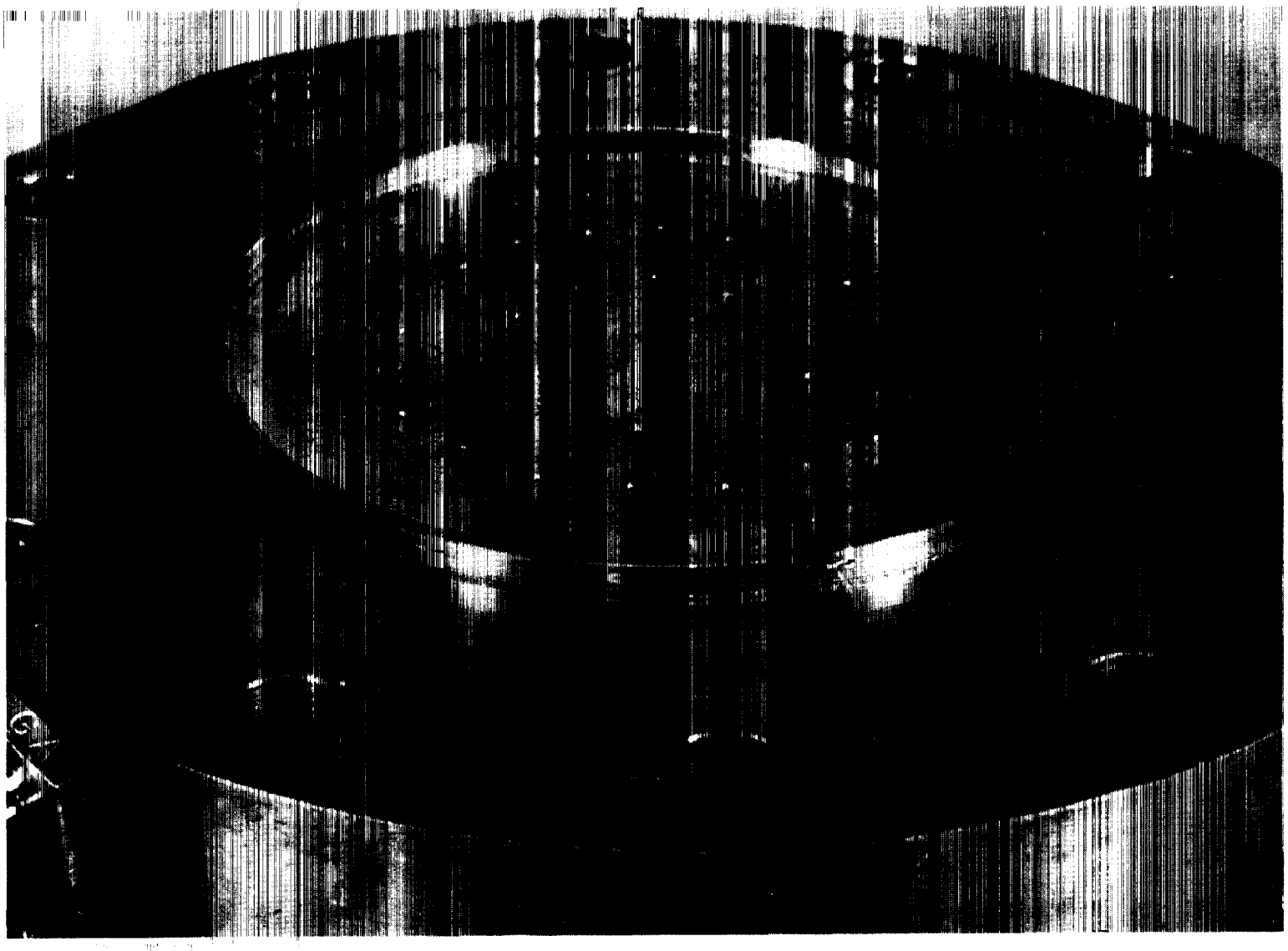

5AJ34-5/8-69-SIA

Figure 30. Swirl Film Cooled Injector Photograph

this value. Mass and mixture ratio distributions as a function of overall mixture ratio are shown in Fig. 31 . This injector was also fabricated from nickel, and EB welded. Instrumentation included manifold pressures and temperatures.

THRUST CHAMBER HARDWARE

The thrust chamber hardware was of heavy wall design, instrumented for longitudinal heat transfer and pressure distribution. Design parameters are shown in Table 4 . Thrust chamber dimensions and instrumentation locations are shown in Fig. 32.

The combustor was selected with the same internal geometry used in the ablative thrust chamber tests on NAS7-304. Heavy wall copper construction was chosen for its large thermal capacity to permit repetitive short tests.

The nozzle is a 15-degree cone and extends from an area ratio of 3.55:1 to an area ratio of 60:1. It is fabricated of mild steel. Thermal instrumentation for the combustor and nozzle are shown in Fig. 43 , and are the same type used in both NASw-1229 and NAS7-304. The thin wafer type is used only in the high area ratio portion of the nozzle.

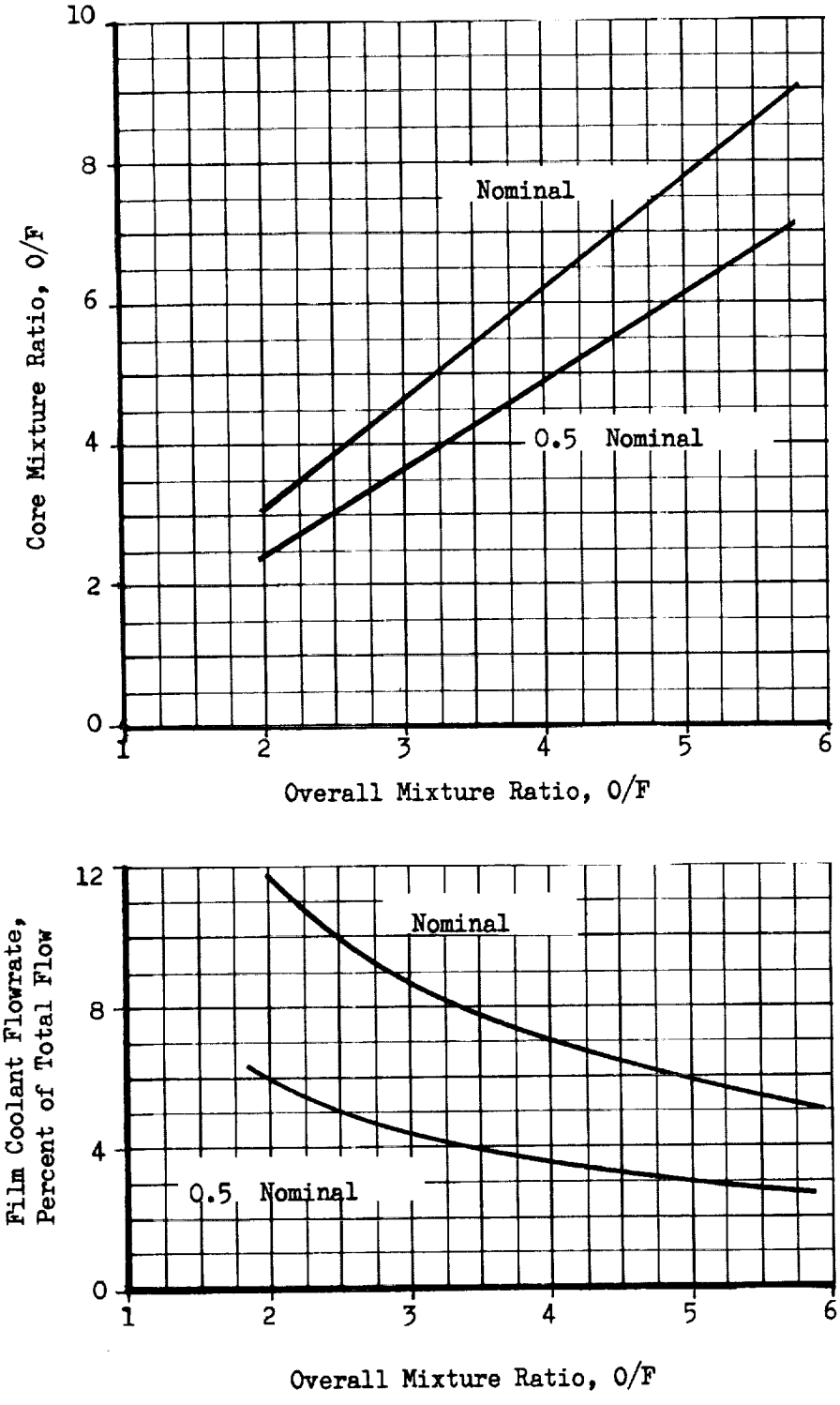


Figure 31. Flow Distribution for Film Cooled Injector

TABLE 4

THRUST CHAMBER DESIGN PARAMETERS

| | |
|---|---|
| Thrust, pounds | 1000 |
| Chamber Pressure, psia | 100 |
| Throat Diameter, inches | 2.54 |
| Chamber Diameter, inches | 3.72 |
| Chamber Contraction Ratio | 2.14:1 |
| Chamber Length, inches | 10.32 |
| Characteristic Length (L*), inches | 20 |
| Throat Convergence Angle, degrees | 11 |
| Throat Radius Ratio, $R/R_T$ | .985 |
| Nozzle Expansion Angle, degrees | 15 |
| Skirt Attach Area Ratio | 3.55 |
| Nozzle Area Ratio | 60:1 |

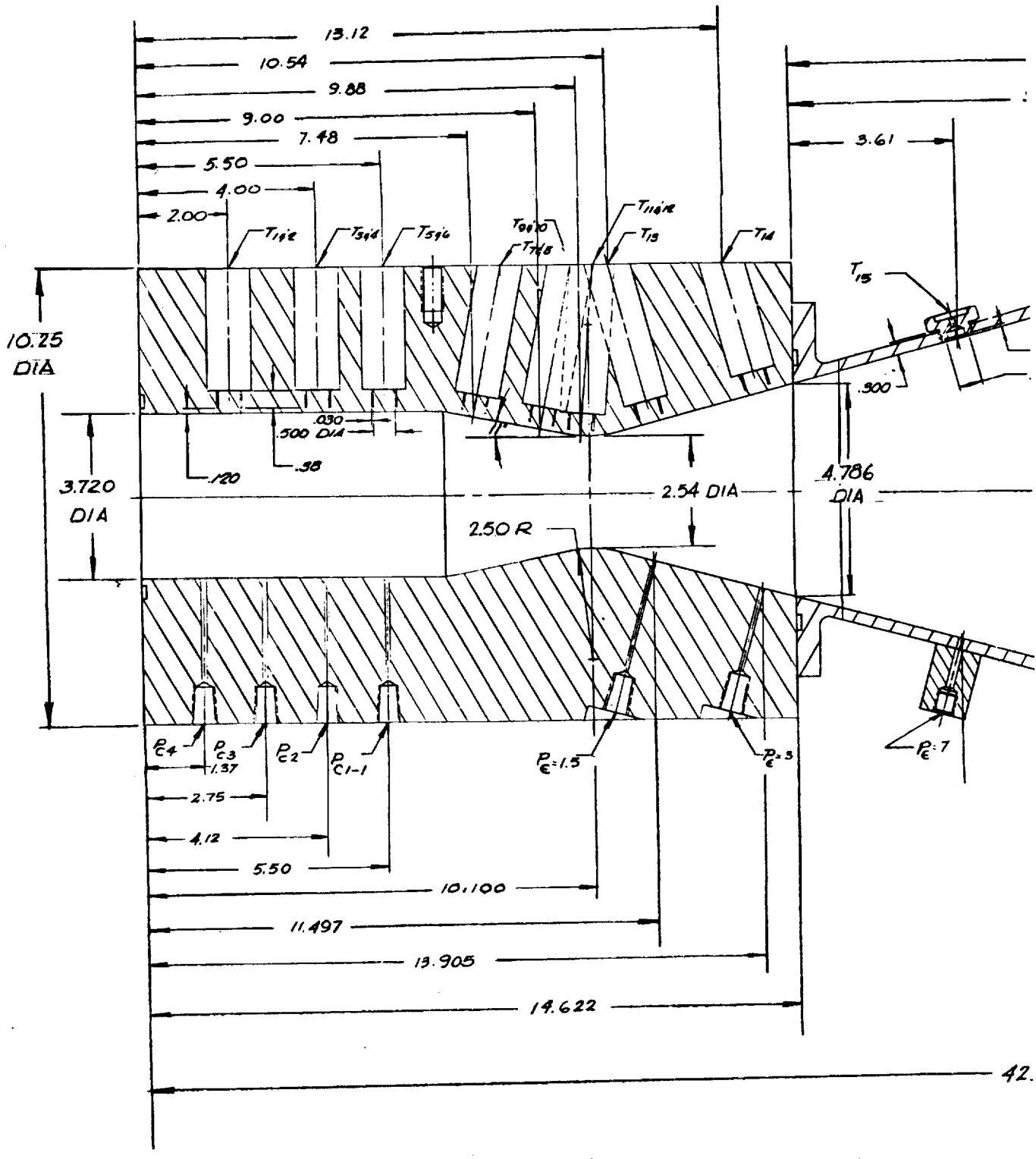


FOLDOUT FRAME

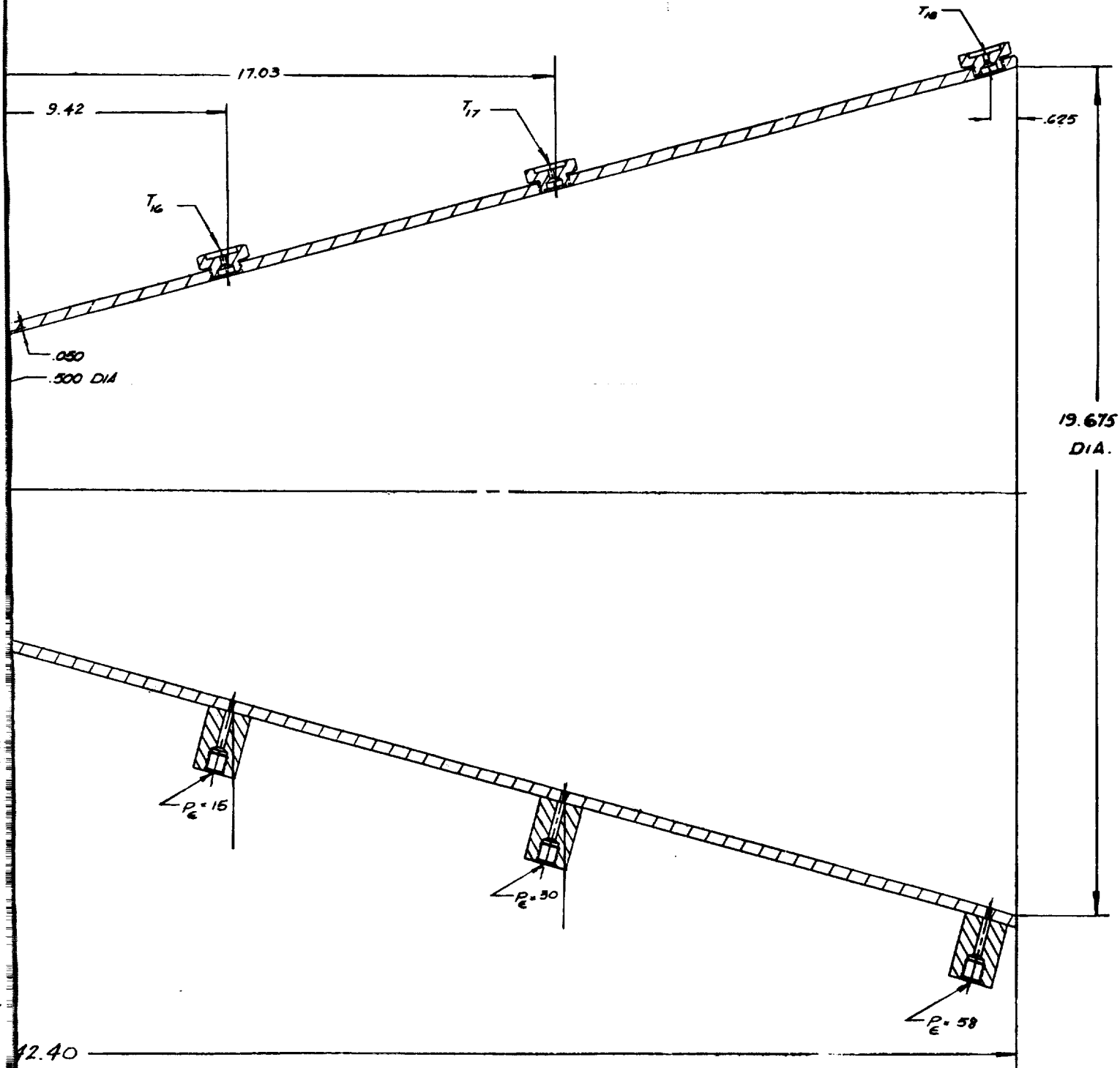


Figure 32. Thrust Chamber Dimensions

FOLDOUT FRAME

## TEST FACILITY

The test program was conducted at the Rocketdyne Nevada Field Laboratory altitude simulation facility B-3 test stand shown in Fig. 33 . This facility produces a simulated altitude of 120,000 feet. The propellant feed system provides both the oxidizer and the fuel as liquids at temperatures controlled by a freon temperature control system. Instrumentation is designed for precise specific impulse performance determination. Specific impulse test results on this facility have consistently been able to resolve performance effects of 1-percent magnitude.

## PROPELLANT SYSTEMS

New features added to the already existing propellant portion of the facility for this program were a liquid diborane run tank and feed system and an $LN_2$-Freon temperature conditioning system for both propellants. Previous tests in this facility had used gaseous diborane at near-ambient temperature and liquid oxidizer at $LN_2$ temperature. A facility flow and valve schematic is shown in Fig. 34 .

### Oxidizer Feed System

The oxidizer feed and storage system is designed for use with any fluorinated cryogenic oxidizer. The storage-test tank is a triple-wall 500-gallon stainless steel tank with a liquid nitrogen inner jacket and an insulation-filled vacuum outer jacket. The tank is shown in Fig. 35 .

The liquid oxidizer system is jacketed and insulated from the test tank to the main valve just upstream of the engine, Fig. 36. The flowmeters are within 4 feet of the injector. Just downstream of the main valve in the oxidizer system, a liquid nitrogen bleed is connected for chilling the injector assembly prior to engine start. A gaseous nitrogen purge is introduced at the same location.

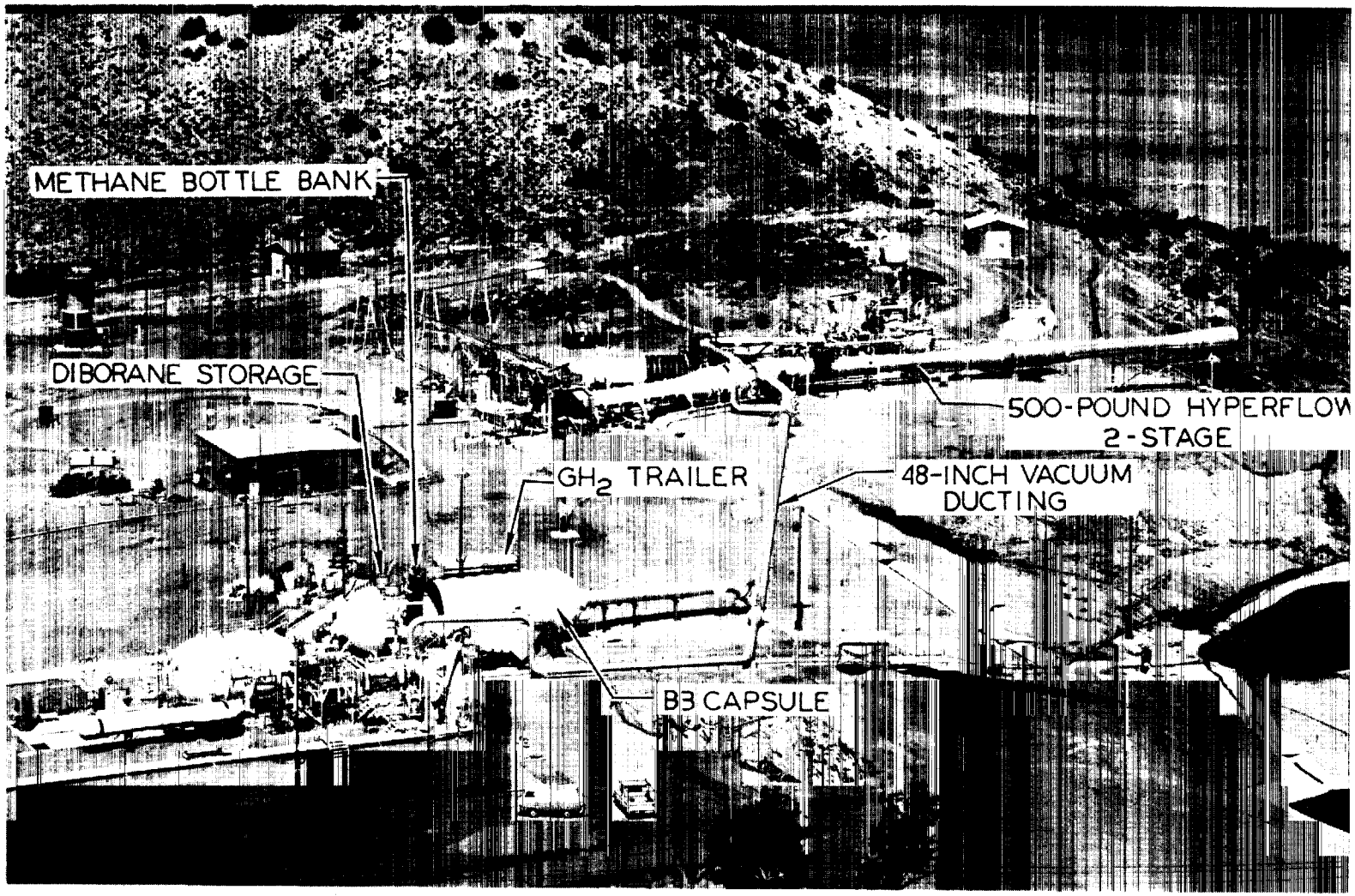


6RE11-3/21/68-R1A

**Figure 33. Nevada Field Laboratory Small Engines Area**

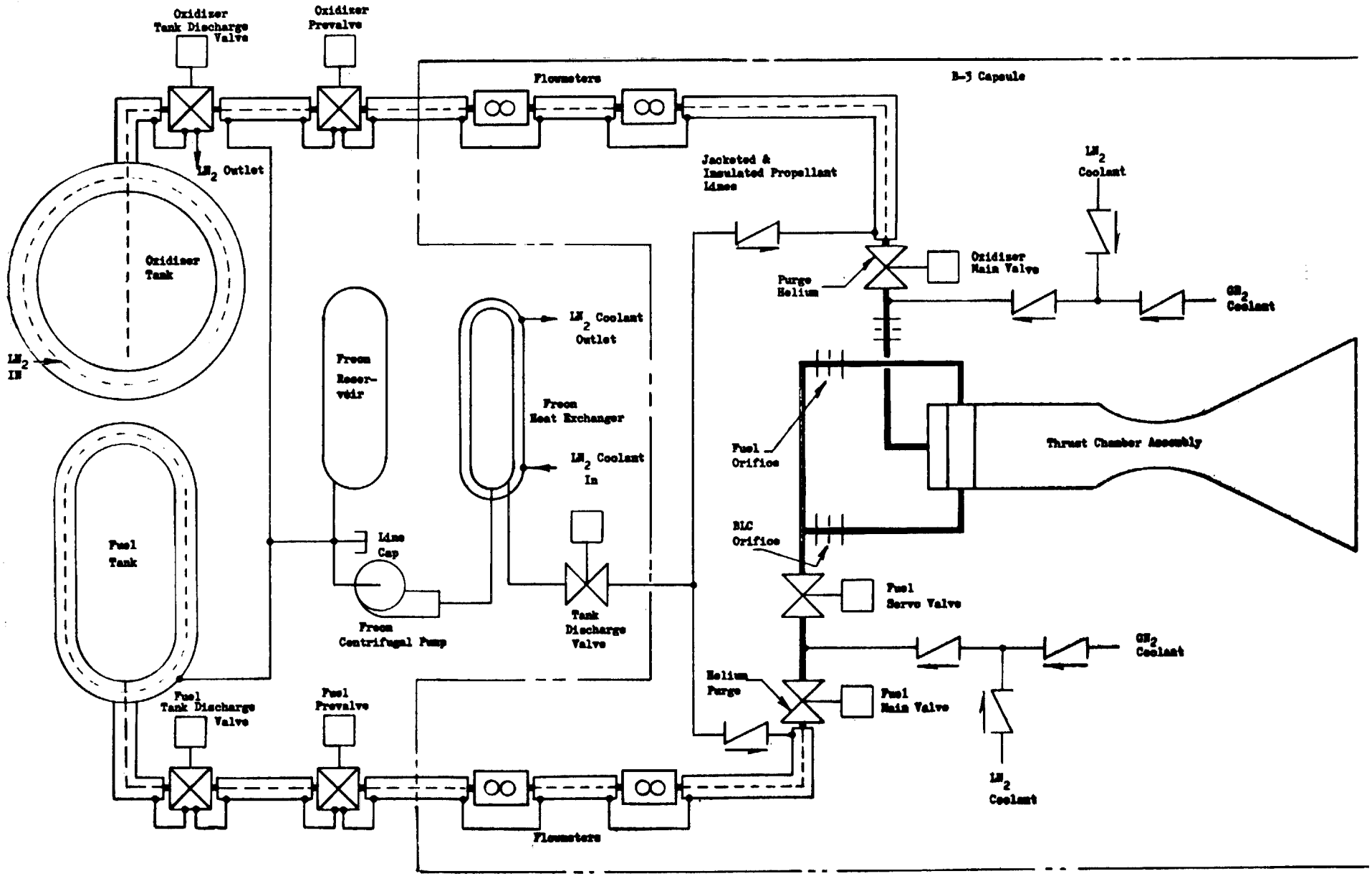


Figure 34. Test Stand Flow Schematic

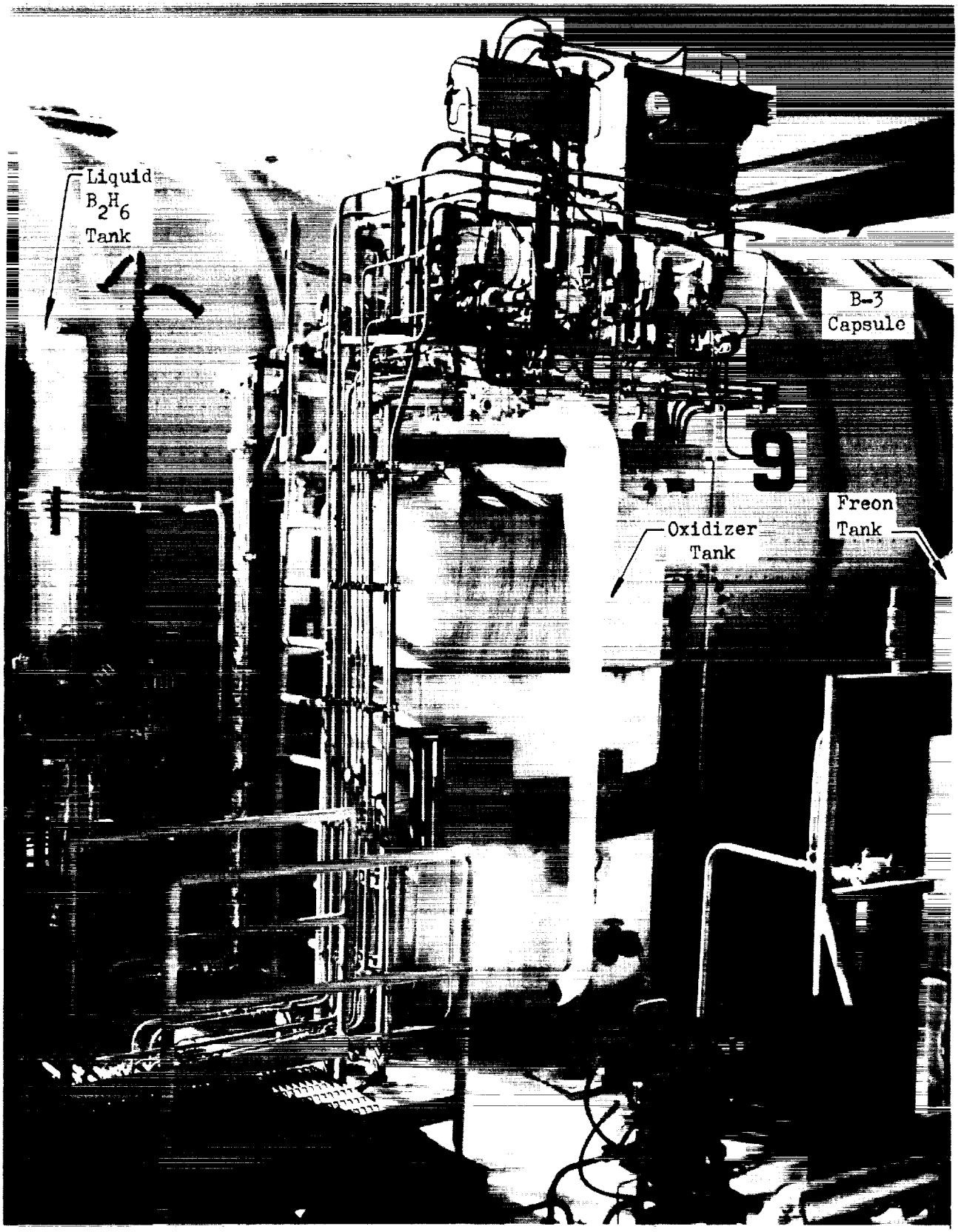


1HZ61-3/6/70-R2B

Figure 35. Oxidizer Storage Area

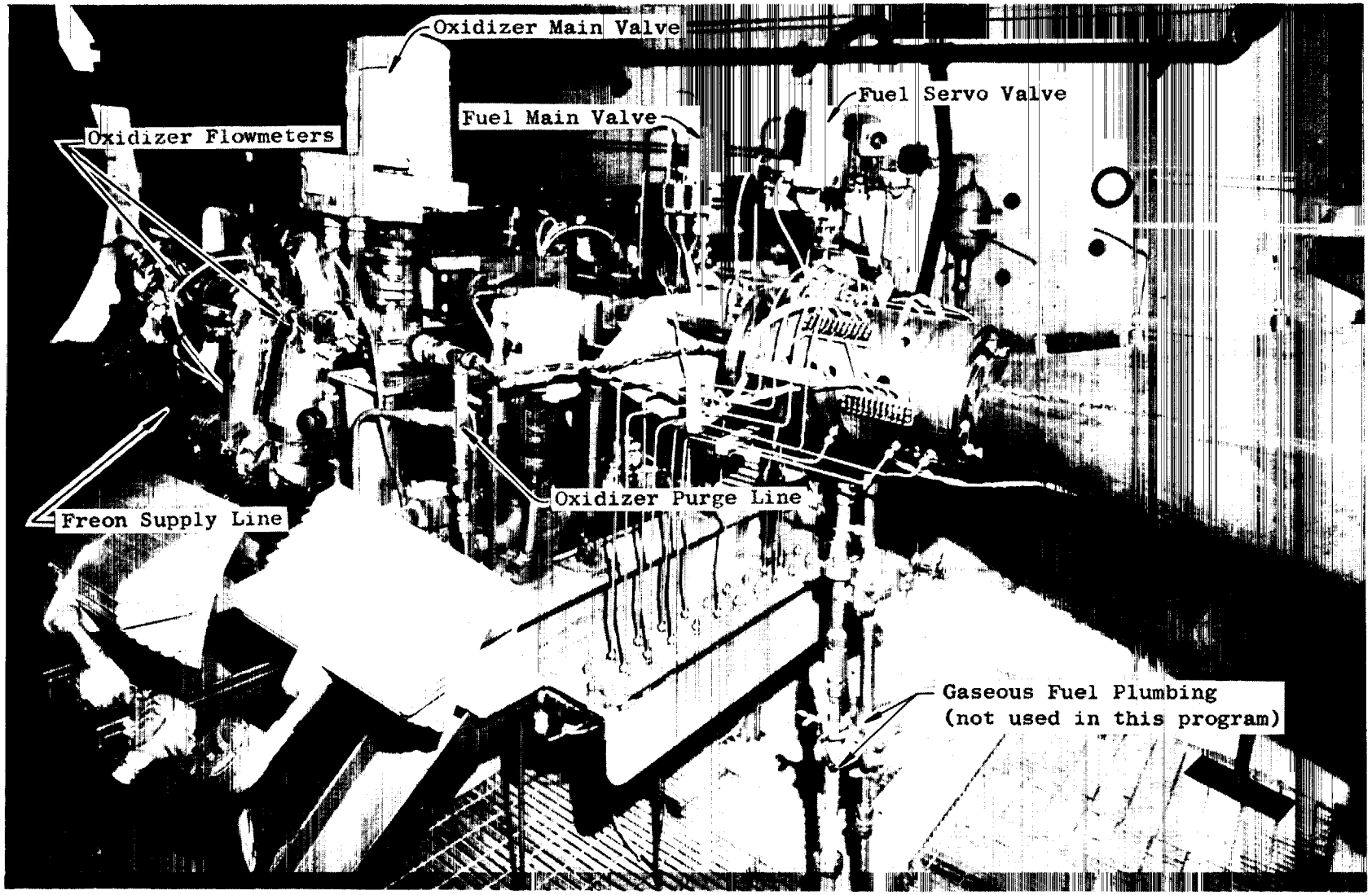


1XW23-10/8/69-R1A

**Figure 36. Oxidizer Feed Lines and Engine Installation**

Except for minor changes in fittings required to switch from $LN_2$ jacketed lines to freon jacketed lines, no modifications were made to the oxidizer system for this program.

Fuel Feed System

The diborane storage system was already in existence at the initiation of this project and required no modification. The liquid storage tank (Fig. 37 ) consists of five toroidal tubes inside an annular container which is used as a jacket. $LN_2$ is sprayed on the top toroidal tube, subsequently dropping to the bottom of the tank where it vaporizes cooling the $B_2H_6$. The $LN_2$ spray flow is regulated to control the $B_2H_6$ storage temperature.

The diborane liquid run tank and jacketed feed lines were added for this program. The run tank is shown in Fig. 38. It has a capacity of 60 pounds of diborane, is cooled by the freon system and is used only during test operations. The liquid feed lines are jacketed and insulated. Two turbine flowmeters are located 6 feet from the engine.

In the activation of the new portions of the diborane facility, a major safety precaution was taken in the use of nontoxic ethane as a simulant for the diborane. The physical properties of the two compounds are close enough that all major facility features could be checked by using ethane. All problems with both the diborane system and the freon system were uncovered using ethane and corrected so that all operations were routine by the time the diborane was first introduced.

Temperature Control System

To satisfy the test objective of using both propellants at the temperatures to be encountered in space, a new temperature control system was added to the facility. This addition consists of a closed loop refrigerated freon system which conditions both propellant feed lines and the fuel run tank. Freon 12 is circulated through cooling jackets and is then, itself, cooled in a liquid nitrogen heat exchanger. The major system components are shown in Fig. 39.

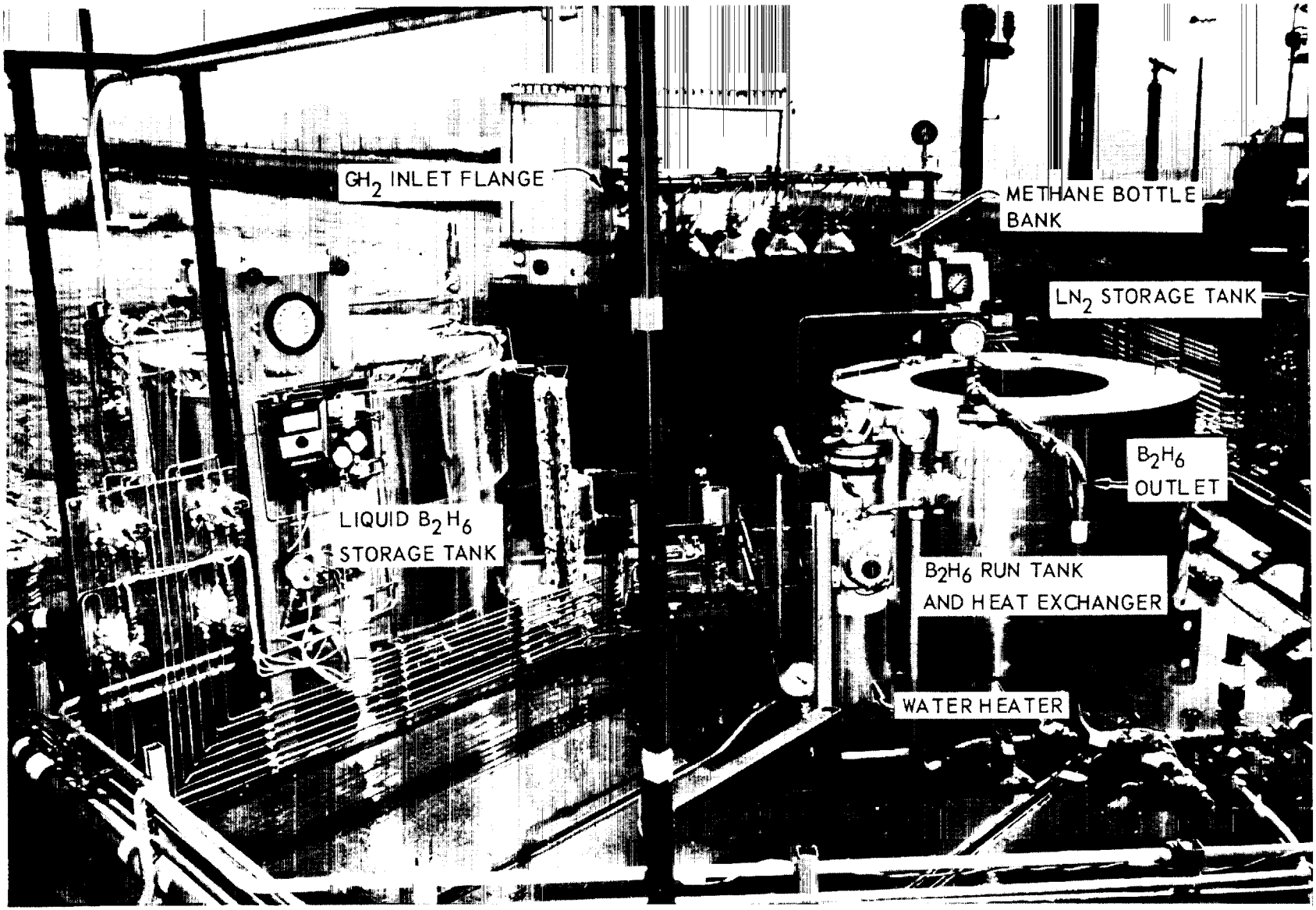


Figure 37. B3 Fuel Storage Area

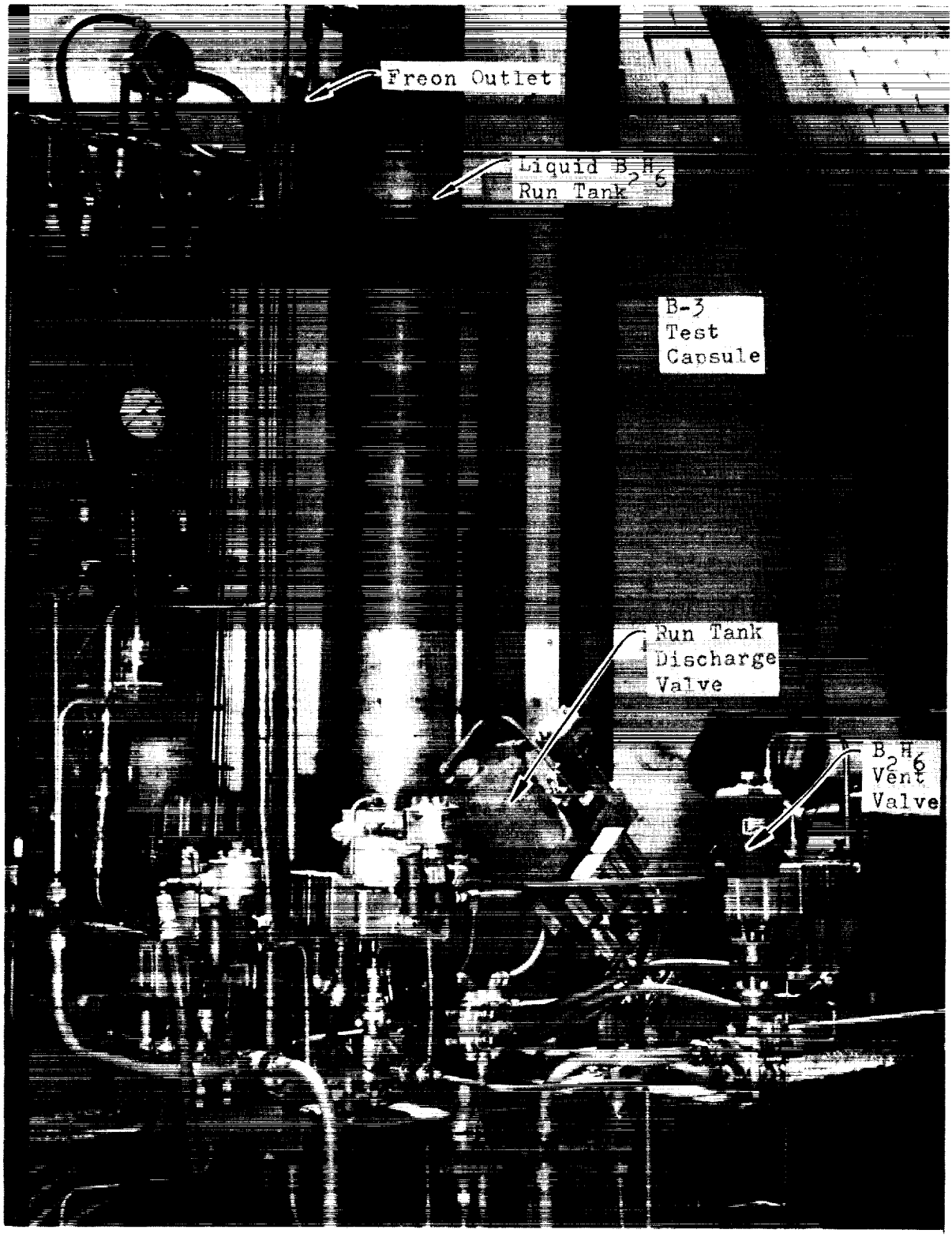


6RB76-7/8-69-RIB

**Figure 38. Diborane Run Tank (Before Insulation)**

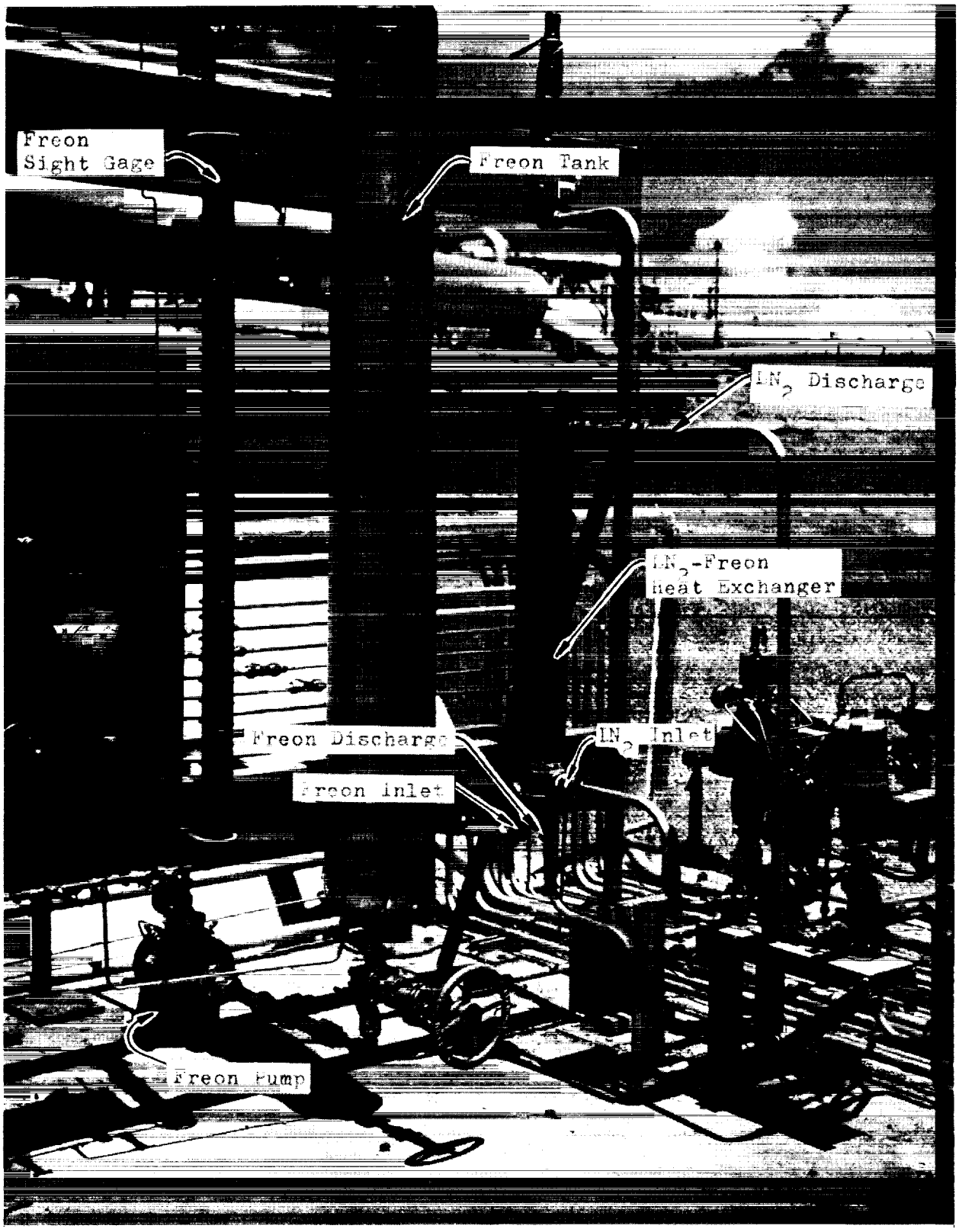


6RB76-7/8/69-RIC

**Figure 39. Freon Refrigeration System (Before Insulation).**

Freon 12 was chosen because of its availability and satisfactory viscosity at operational conditions. The freon 12 has a freezing point about -252°F, very similar to that of diborane. A centrifugal chemical pump was chosen for circulating the freon. The only pump modification required was the removal of the oil in the coolant sump, to permit use at cryogenic temperature. The heat exchanger is a series of tubes manifolded on each end and cooled with $LN_2$. The operational system currently takes approximately 30 minutes to stabilize.

## ALTITUDE SIMULATION SYSTEM

A twofold altitude-simulation system was used in this program, the main system, consisting of three diffuser stages, is capable of maintaining an altitude of 120,000 feet for 150 seconds of test operation. The first stage is driven by the engine, while the other two stages are powered by supersonic steam ejectors. The overall system is shown in Fig. 33.

The auxiliary ejector unit is supplied by steam from the main boiler plant. This ejector, although not capable of maintaining altitude conditions during test operation, permits evacuation and facility checkout before starting the large system.

The altitude test capsule consists of a cylinder approximately 16 feet in diameter and 40 feet long with hemispherical ends. The aft end is connected to the altitude-simulation system by a 48-inch duct. The forward end of the capsule is mounted on a movable trolley for access. The opened capsule is shown in Fig. 33. The ducting leading to the main ejectors and the isolation valves are also evident in this figure.

## ENGINE INSTALLATION

The engine is installed in the test stand in such a way that external interference is minimized, and thrust is calibrated with all plumbing in place. Thus, no corrections have to be made to thrust for resistance caused by supports or propellant lines. The diffuser inlet is adjusted to ensure that there is no effect of the engine plume within the capsule.

## Engine Mounts

The thrust system is illustrated in Fig. 40. The injector (not shown)is mounted to the thrust plate by three longitudinal standoffs. This plate is supported by one horizontal and two vertical tie rods. Mounted to the thrust plate is a flexure and spacer followed by a dual-bridge load cell. Two alignment plates separate the two load cells and flexures. This assembly is mounted to a rigid I-beam. Also mounted to this I-beam is a hydraulic ram and the calibration load cell. At the end of the calibration cell is a ball joint in a yoke that is tied to the thrust plate by two tension rods. To minimize the cantilevered engine weight, a vertical rod and a horizontal rod are attached to the nozzle skirt, Fig. 41.

The engine thrust is simulated for calibration by pressurizing the hydraulic ram which moves the calibration cell putting the two tie rods in tension. In this manner, the simulated engine thrust is transmitted through the centerline of the thrust system putting the dual-bridge load cells in compression in the same manner realized during engine operation. During test operation the tie rods are loosened and do not interfere with engine movement.

## Propellant Lines

The engine plumbing consists of instrumentation lines and propellant feed lines. To minimize test stand effect, all the propellant plumbing is introduced to the injector with relatively long radial straight sections to allow unrestrained movement of the chamber assembly. The engine instrumentation also has the same feature. The instrumentation lines are "S" shaped with long leg sections and are fabricated from 1/4-inch light wall tubing. There is no insulation or jacketing on any lines downstream of the rigidly mounted valves or transducers.

## Diffuser

The diffuser extension (Fig. 41) is 25 inches in diameter. When the 15 degree conical hardware is installed in the stand, the nozzle protrudes into the diffuser approximately two inches.

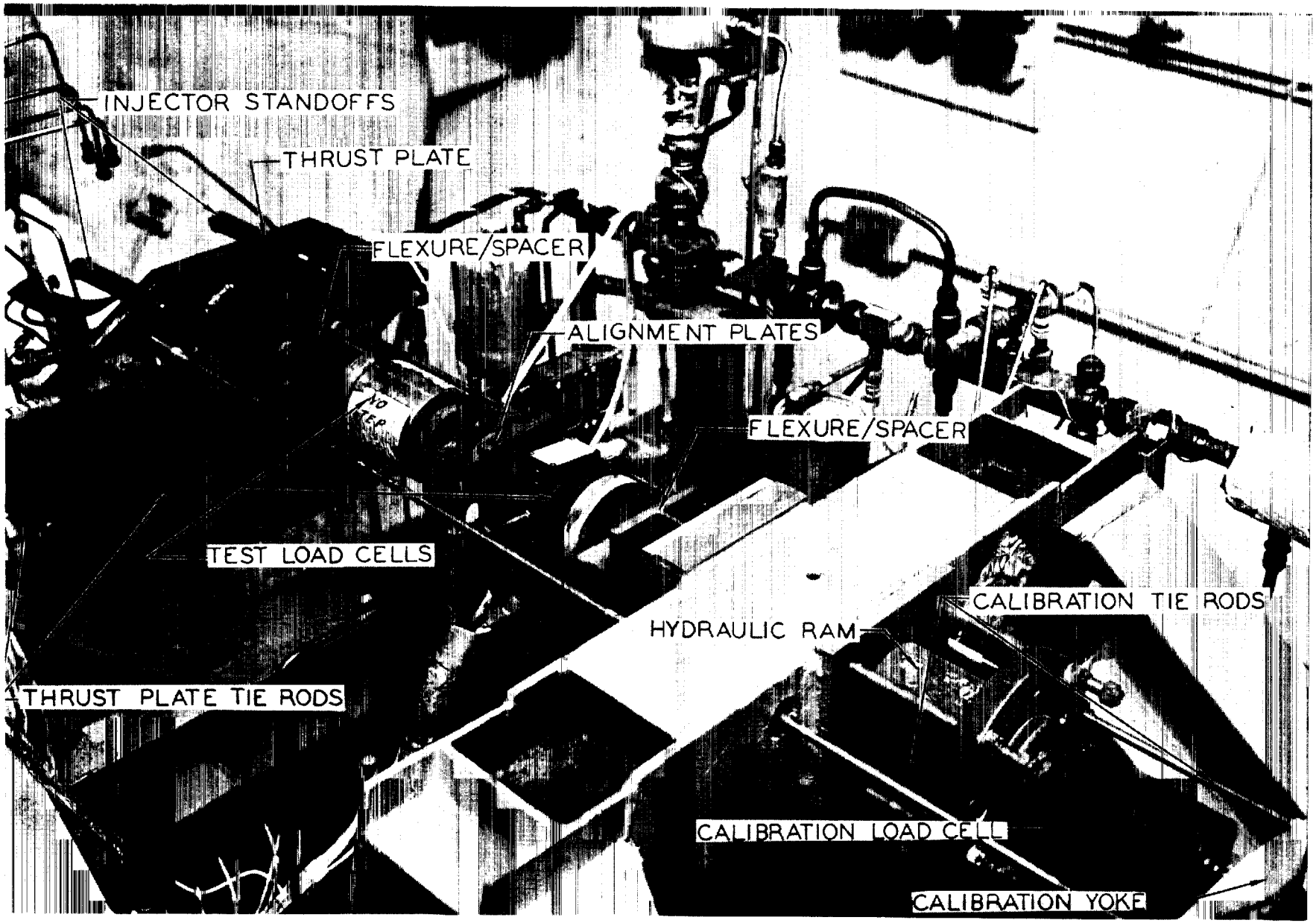


**Figure 40. Engine Thrust Mount System**

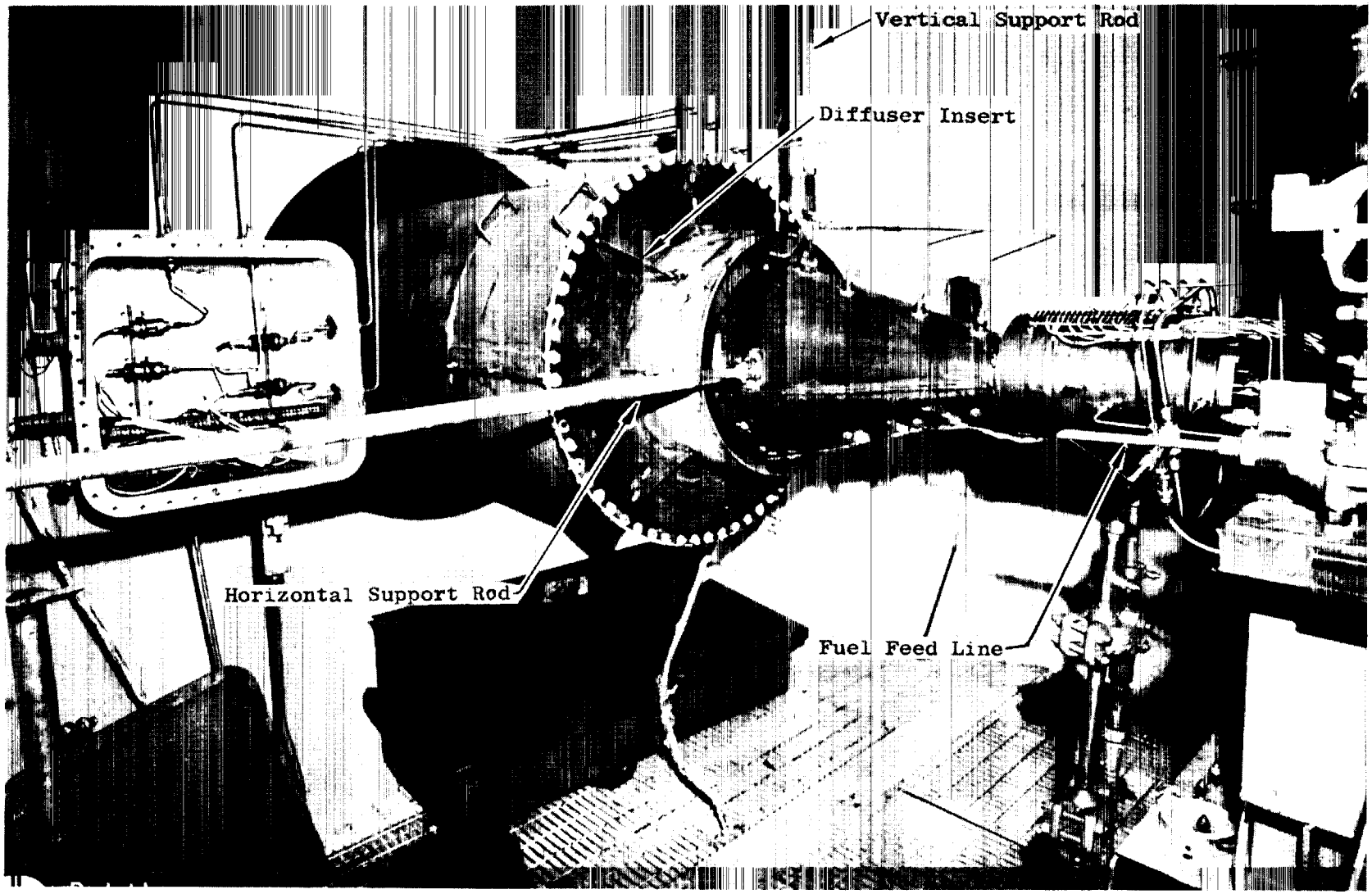


1XW23-10/8/69-R1B

**Figure 41. Engine Installation and B-3 Capsule Interior**

## INSTRUMENTATION

In this program, the test objective has been the acquisition of high quality data. Therefore, special emphasis was placed upon instrumentation and instrumentation systems. Because certain parameters are critical in determining engine performance (e.g., flowrates, thrust and chamber pressure) the critical items in these measurements were made redundant.

The location of major test stand instrumentation is shown schematically in Fig. 42. The exact location of the thrust chamber instrumentation is shown in Fig. 32.

### Data Acquisition System

Primary data acquisition was by digital recorder. This digital unit is an Astrodata Model 4024 system with 88 active channels, 12 FM-DC flow channels and 64 event channels. A sampling rate of 20,000 samples/sec was used, with a sampling time of approximately 12 milliseconds. The Astrodata unit is coupled to an on-site DDP 116 computer which was used to obtain scaled engineering data and limited on-site data reduction.

### Thrust Measurement

Thrust measurement is made by two-series Baldwin-Lima-Hamilton double-bridge load cells. Each cell provides a redundant measurement by the double-bridge network, resulting in four separate thrust measurements. Calibration of the load cells is conducted before and after each test series by means of the calibration load cell and a hydraulic loader, Fig. 40. The calibration load cell is calibrated against a proving ring traceable to the National Bureau of Standards.

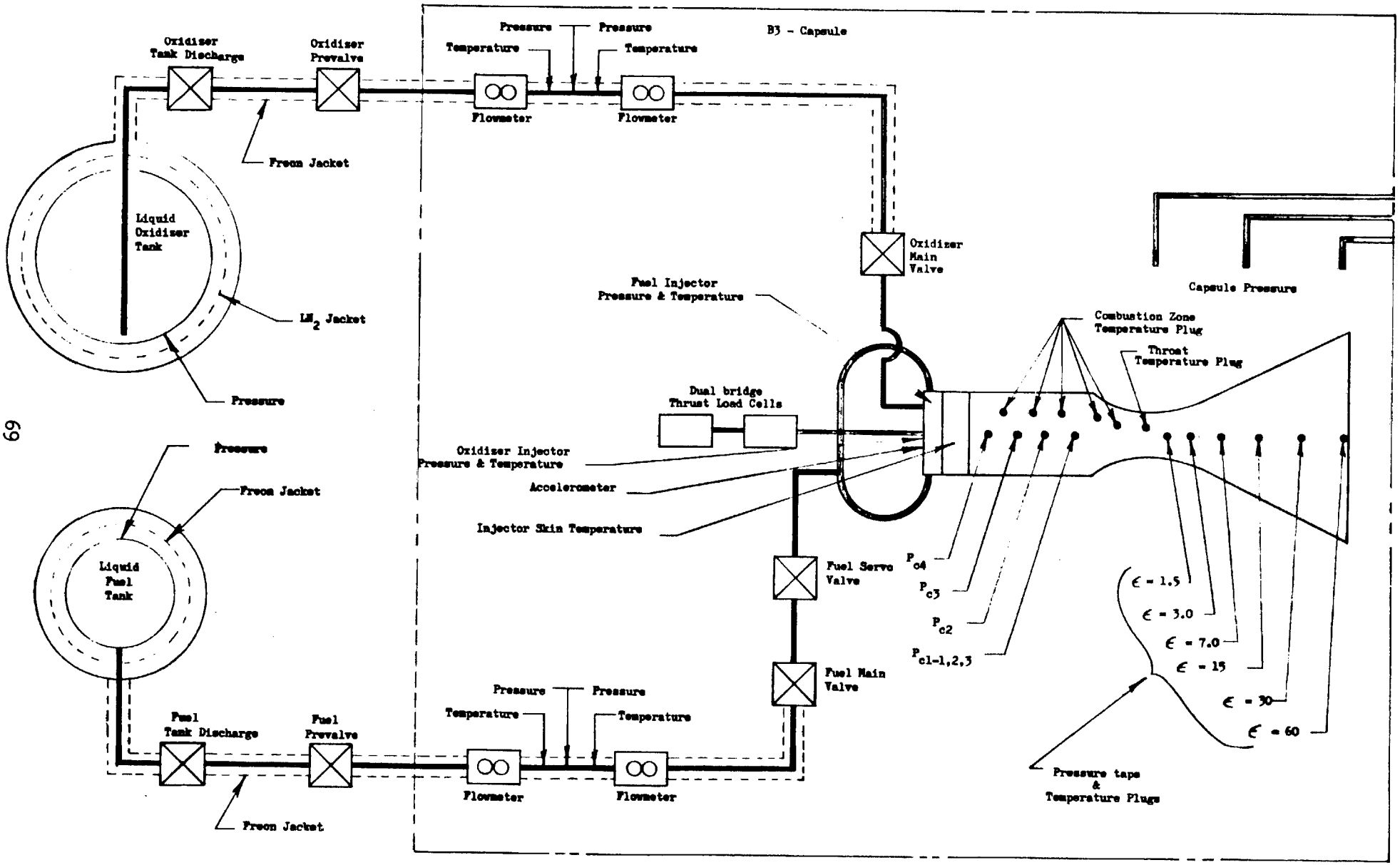


Figure 42. Test Stand Instrumentation Schematic

## Pressure Measurement

Pressure transducers are of the bonded strain gage, d-c type. The calibration and verification of the pressure transducers are accomplished with a dead weight tester or similarly precise calibration device traceable to the National Bureau of Standards. For LOX clean certified pressure transducers, the calibration and verifications are accomplished by introducing $GN_2$ and measuring the pressure on a Heise gage.

## Flow Measurement

Propellant flowrate is measured using redundant turbine-type volumetric flowmeters, Fig. 36. These meters were calibrated using liquid freon.

## Temperature Measurements

Propellant temperature is measured using Rosemount shielded platinum resistance bulbs, immersed in the liquid stream. Iron constantan thermocouples are used for the major portion of the thrust chamber temperatures used in the heat transfer calculations. Chromel-Alumel thermocouples are used where higher temperatures are anticipated.

## Heat Flux Measurement

Heat flux determination is based upon the temperature-time history of special control sections embedded in the thrust chamber wall. The temperature measuring device consists of a thermal isolation segment with a thermocouple located on the back side of the segment. The isolation segments used in the test program are of two types. These are depicted in Fig. 43. Type (a) is installed in the combustor, throat, and low area ratio regions to measure high heat flux levels, whereas Type (b) is installed in the nozzle section where heat flux is low. Type (a) is made by cutting isolation grooves into the copper wall to reduce three dimensional heat transfer effects. (However, the remaining effects are still accounted for analytically in the data reduction). Thermal

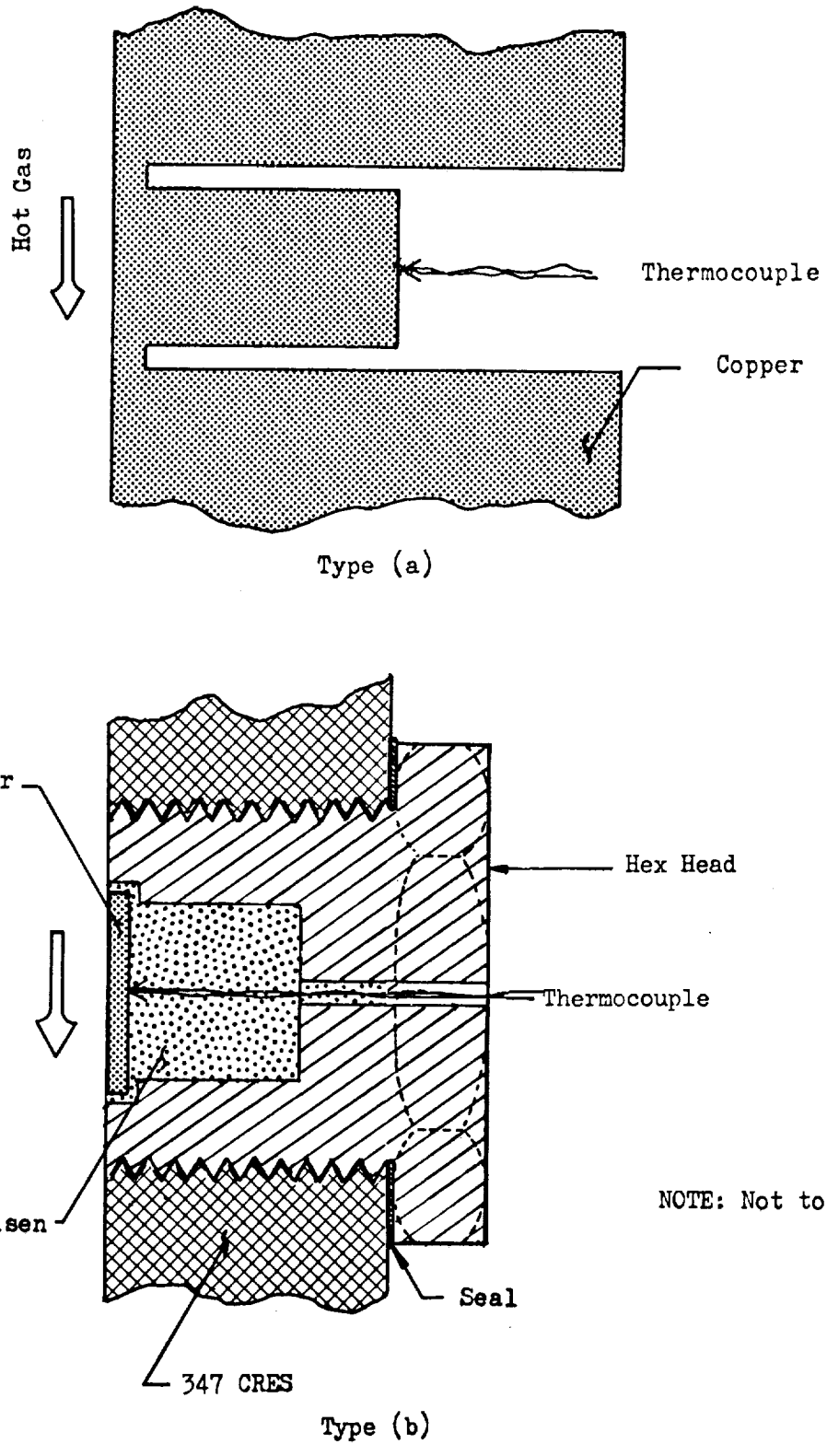


Figure 43. Schematic Cross-Sections of Heat Transfer Isolation Segments

plug Type (b) is made by inserting steel plugs into the steel nozzle wall. Each plug contains a thin copper wafer to which is bonded a thermocouple. In this way, heat loss from the plug is minimized and the maximum possible temperature response is obtained.

# DATA INTERPRETATION PROCEDURES

Several terms are used in this report to describe the experimental results. To ensure the reader's ability to understand these results, this section contains descriptions of the calculations used in the data interpretation. The details of recording, averaging and converting the digital data to give engineering values of each parameter are straightforward and are not discussed. The details of converting the measured engineering parameters to performance parameters are of interest in that the manner of accounting for some effects can make a significant difference in the calculated results.

## PERFORMANCE DATA

Three terms are used in this report to describe performance. Specific impulse is defined as vacuum thrust divided by flowrate. No corrections are included in specific impulse results any place in this report. For indication of loss modes, an injector efficiency is defined which includes all losses caused by the nonideal combustion chamber and injector. The injector efficiency is the value of characteristic velocity efficiency that would have been achieved if the combustion chamber had been insulated, frictionless and one dimensional, and is defined on page 74. The thrust chamber efficiency is defined as the ratio of specific impulse efficiency to the injector efficiency.

It is not possible to present the ICRPG preferred energy release efficiency (Ref. 5) for this program because no low area ratio tests were conducted and because the large mixture ratio striation and film coolant cause the assumption of no mixing between streamtubes to be invalid.

### Performance Calculation

For data evaluation, a rocket thrust chamber performance model was assumed which, in accordance with Ref. 5, categorizes performance losses into:

1. Heat transfer to chamber and injector upstream of boundary layer attachment point.
2. Mixture ratio distribution (streamtubes).
3. Energy release.
4. Finite reaction rate. (kinetics)
5. Two-dimensional flow.
6. Boundary layer. (friction and heat transfer)
7. Two-phase flow - not considered at present.

These loss mechanisms have effects on both specific impulse and characteristic velocity.

Specific impulse efficiency as presented in this report contains no corrections to the experimental data and reflects the combined losses due to all of the mechanisms listed above.

The term injector efficiency is defined

$$\eta_{inj} = \frac{P_c A_t g \left(1-2\frac{\Delta_t^*}{R_t}\right)\left(\frac{\dot{m}_{2D}}{\dot{m}_{1D}}\right)}{C^*_{ideal}\ \dot{W}_{Total}} + \left(1-\eta_{HL_{C^*}}\right)$$

where

$\Delta_t^*$ = boundary layer displacement thickness at the throat

$R_t$ = throat radius

$\frac{\dot{m}_{2D}}{\dot{m}_{1D}}$ = potential flow discharge coefficient

$1-\eta_{HL_{C^*}}$ = $C^*$ inefficiency due to heat loss to the chamber wall upstream of the point of boundary layer initiation.

Thus, injector efficiency represents the combined losses in $C^*$ as a result of finite reaction rates, mixture ratio distribution and incomplete energy

release. For a chemically uniform flow in chemical equilibrium flowing through a real nozzle throat the injector efficiency would be 100 percent.

In this formulation, losses due to heat transfer upstream of the boundary layer are corrected for and charged to the thrust chamber instead of the injector. However, in this program the heat loss was small and was ignored.

The thrust chamber efficiency is defined as:

$$\eta_{TC} = \frac{\eta_{I_s}}{\eta_{inj}}$$

and represents the losses due to all effects not included in the injector efficiency. The thrust chamber efficiency contains the effects of many interacting loss modes (e.g., kinetics, divergence, boundary layer, striations, mixing, etc.) which are not well understood for $OF_2/B_2H_6$. This empirical term will be very useful until suitable analytical techniques become available for this propellant.

The division of losses between $\eta_{inj}$ and $\eta_{TC}$ depends on the ability to deduce average stagnation pressure and aerodynamic throat area from test measurements. In these tests, where the flow was highly nonuniform and the contraction ratio was low, these values should be used with caution.

Thrust Data

The vacuum thrust was calculated by averaging the four thrust measurements and correcting for ambient pressure by:

$$F_{vac} = F_{avg} + P_a A_e$$

Because all tests were conducted at low environmental pressure, the correction term was small (2 to 3 percent) compared to the total; therefore, small errors for base effects or small errors in pressure or area are negligible.

No other corrections are necessary because the test stand design and calibrating procedures are such that corrections for external loads on the engine are eliminated.

## Flowrate Data

For the flowmeters, pressure, temperature and rotational frequency are recorded. Propellant flowrate is found from the liquid pressure and temperature, and rotational frequency of the flowmeter. The viscosities of the liquid propellants are found from the pressure and temperature. Density is computed from the pure propellant properties and corrected for the exact composition. The rotational frequency is corrected for the difference in viscosity between calibration and test fluids by dividing the frequency by the kinematic viscosity. The conversion from corrected frequency to gallons per second is found from the flowmeter calibration curve. This value is finally corrected for flowmeter shrinkage from the calibration temperature to the propellant temperature.

## Throat Area

Because the hardware increases in temperature continuously during a test series, a correction must be applied to account for hardware throat growth prior to each test. Transient analysis for the test duration and chamber design used indicate no physical throat area change during the tests. The pretest throat area ($A_t$) is then corrected for aerodynamic and boundary layer discharge coefficients to give the actual available flow area ($A^*$). The discharge coefficient used was:

$$\left(1 - 2\frac{\Delta^* t}{R_t}\right)\left(\frac{\dot{m}_{2D}}{\dot{m}_{1D}}\right) = 0.9926$$

## Chamber Pressure

The chamber pressure (throat stagnation pressure) is calculated from the wall static pressure measured prior to start of contraction but after all major combustion has taken place. The wall static pressure was assumed

equal to the core static pressure. The core static pressure is then corrected to a throat stagnation pressuring using the isentropic relationship.

$$\frac{P_c}{P_{static}} = \left(1 + \frac{n-1}{2} M^2\right)^{\frac{n}{n-1}}$$

where the n used is a process exponent for the equilibrium expansion and not the local specific heat ratio. The ratio of stagnation to static pressure used was 1.0485.

Correction for Impurities

All currently available propellants have some minor amount of impurities. The areas affected by the impurities are the flowrates and the combustion and expansion processes. The flowrates are adjusted by taking into account the actual densities. The combustion and expansion processes are less efficient than for pure propellants, but because the objective of this program was to determine deliverable performance, and because the propellants were of good quality (Table 5) no corrections were made for theoretical effects.

HEAT TRANSFER DATA

Heat transfer data were taken using thermal isolation sections as described in Fig. 43. The resultant data were in the form of temperature-time histories. When nondimensionalized, these histories were compared with results of a one dimensional transient heat conduction model to establish the heat flux.

The theoretical, nondimensional, back side wall temperature-time histories were obtained from a transient heat conduction analysis assuming an infinite plate solution with one surface exposed to the combustion gas and the other surface insulated. The assumption of the infinite plate (one-dimensional conduction) is reasonable because of the insulating effects of the air

and/or 347 stainless steel that surrounds the measuring plug. Small corrections are made for the true geometry of the plugs where necessary to reduce the test data to infinite plate form.

Test results are presented as heat flux values and are therefore applicable to other configurations where wall temperatures are similar to the moderate values encountered in this test program. Extrapolation to high wall temperature requires knowledge of adiabatic wall temperature and the boundary layer film coefficient, both of which are uncertain for stratified or film cooled test configurations.

All heat flux results were modified by the ratio $(100/P_c)^{0.8}$ to correct data to the nominal 100 psia conditions.

TABLE 5 PROPELLANT CHEMICAL ANALYSIS RESULTS

Oxygen Difluoride

| Constituent | Mole % | Weight % |
|---|---|---|
| $OF_2$ | 98.9 | 99.2 |
| $N_2$ | 0.6 | 0.3 |
| $CF_4$ | 0.2 | 0.3 |
| He | 0.1 | < 0.1 |
| $CO_2$ | 0.1 | 0.1 |
| Ar | < 0.1 | < 0.1 |

Diborane

| | | |
|---|---|---|
| $B_2H_6$ | 97.1 | 99.6 |
| $H_2$ | 2.7 | 0.2 |
| $N_2$ | 0.2 | 0.2 |

Note: Higher boranes below level of detection with infrared spectrum

## REFERENCES


1. R-7985, Chamber Technology for Space Storable Propellants, Fourth Interim Report for the Period 29 June 1967 through 26 August 1969, Rocketdyne, a Division of North American Aviation, Inc., Canoga Park, California, September, 1967.

2. Report 659-F, FLOX-Diborane Technology - Boundary Reactions, Aerojet-General Corporation, Sacramento, California, September 1969.

3. Report RMD 6028-F, Investigations of Space Storable Propellants, Thiokol Chemical Corporation, Reaction Motors Division, Denville, New Jersey, January 1964.

4. R-6696-3, Fluorine-Hydrogen Performance Evaluation, Phase II: Space Storable Propellant Performance Investigation, Final Report, Rocketdyne, a Division of North American Aviation, Inc., Canoga Park, California, April, 1969.

5. CPIA No. 178, ICRPG Liquid Propellant Thrust Chamber Performance Evaluation Manual, September, 1968.